

TIME-SERIES PHOTOMETRY OF GLOBULAR CLUSTERS: M62 (NGC 6266), THE MOST RR LYRAE-RICH GLOBULAR CLUSTER IN THE GALAXY?

R. CONTRERAS,^{1,2} M. CATELAN,² H. A. SMITH,³ B. J. PRITZL,⁴ J. BORISSOVA,⁵ C. A. KUEHN³

AJ, in press

ABSTRACT

We present new time-series CCD photometry, in the *B* and *V* bands, for the moderately metal-rich ($[\text{Fe}/\text{H}] \simeq -1.3$) Galactic globular cluster M62 (NGC 6266). The present dataset is the largest obtained so far for this cluster, and consists of 168 images per filter, obtained with the Warsaw 1.3m telescope at the Las Campanas Observatory (LCO) and the 1.3m telescope of the Cerro Tololo Inter-American Observatory (CTIO), in two separate runs over the time span of three months. The procedure adopted to detect the variable stars was the optimal image subtraction method (ISIS v2.2), as implemented by Alard. The photometry was performed using both ISIS and Stetson's DAOPHOT/ALLFRAME package. We have identified 245 variable stars in the cluster fields that have been analyzed so far, of which 179 are new discoveries. Of these variables, 133 are fundamental mode RR Lyrae stars (RRab), 76 are first overtone (RRc) pulsators, 4 are type II Cepheids, 25 are long-period variables (LPV), 1 is an eclipsing binary, and 6 are not yet well classified. Such a large number of RR Lyrae stars places M62 among the top two most RR Lyrae-rich (in the sense of total number of RR Lyrae stars present) globular clusters known in the Galaxy, second only to M3 (NGC 5272) with a total of 230 known RR Lyrae stars. Since this study covers most but not all of the cluster area, it is not unlikely that M62 is in fact the most RR Lyrae-rich globular cluster in the Galaxy. In like vein, thanks to the time coverage of our datasets, we were also able to detect the largest sample of LPV's known so far in a Galactic globular cluster.

We analyze a variety of Oosterhoff type indicators for the cluster, including mean periods, period distribution, Bailey diagrams, and Fourier decomposition parameters (as well as the physical parameters derived therefrom). All of these indicators clearly show that M62 is an Oosterhoff type I system. This is in good agreement with the moderately high metallicity of the cluster, in spite of its predominantly blue horizontal branch morphology – which is more typical of Oosterhoff type II systems. We thus conclude that metallicity plays a key role in defining Oosterhoff type. Finally, based on an application of the “A-method,” we conclude that the cluster RR Lyrae stars have a similar He abundance as M3, although more work on the temperatures of the M62 RR Lyrae is needed before this result can be conclusively established.

Subject headings: stars: horizontal-branch – stars: variables: other – Galaxy: globular clusters: individual (M62, NGC 6266)

1. INTRODUCTION

By the early 1990's, it was widely perceived that “most variable stars that belong to Galactic globular clusters have by now been discovered” (Suntzeff et al. 1991). Indeed, Suntzeff et al. estimated that only a few percent of the total population of RR Lyrae variable stars remained to be discovered in globular clusters. However, most of the pre-1990 studies based their results on photographic photometry, which in many cases appears not to have been precise enough to detect small-amplitude variables. On the other hand, new techniques, based on image subtraction algorithms, have been developed in the last years, which are capable of quickly, efficiently and automatically detecting star variations even in the most crowded fields (e.g., Alard 2000; Bramich 2008). In fact, several studies have reported substantial in-

creases in the reported globular cluster RR Lyrae populations using these techniques (e.g., Kaluzny, Olech, & Stanek 2001; Corwin et al. 2004; Zorotovic et al. 2009). It seems that, contrary to what was previously thought, the sample of RR Lyrae variables identified so far in Galactic globular clusters is significantly incomplete, thus rendering further analyses, based on high-quality CCD observations and image subtraction techniques, well worth the while.

NGC 6266 (M62) is a high-density ($\log \rho_c = 5.34 L_\odot \text{pc}^3$), highly reddened [$E(B-V) = 0.47$] cluster, and is also one of the most massive in our galaxy, with $M_V = -9.19$ (Harris 1996). Located at just 1.7 kpc from the Galactic center, it has also been classified as a possible post-core collapse globular cluster by Trager, Djorgovski, & King (1993, 1995) – a possibility which however was not confirmed by Beccari et al. (2006) in their study of the radial density profile of the cluster. Also worth mentioning is the fact that the cluster currently ranks fifth in the number of millisecond pulsars (Cocozza et al. 2008, and references therein).

The morphology of the cluster's horizontal branch (HB) shows a prominent blue component, in addition to a very extended blue tail, reaching down to at least the main sequence turnoff level (e.g., Caloi et al. 1987; Piotto et al. 2002). The cluster is also known to be rich in RR Lyrae variables (Clement et al. 2001, and references therein). These features are strikingly similar to those of M15 (NGC 7078), perhaps

¹ INAF-Osservatorio Astronomico di Bologna, via Ranzani 1, 40127, Bologna, Italy

² Pontificia Universidad Católica de Chile, Departamento de Astronomía y Astrofísica, Av. Vicuña Mackenna 4860, 782-0436 Macul, Santiago, Chile

³ Department of Physics and Astronomy, Michigan State University, East Lansing, MI 48824

⁴ Department of Physics and Astronomy, University of Wisconsin, Oshkosh, WI 54901

⁵ Departamento de Física y Astronomía, Facultad de Ciencias, Universidad de Valparaíso, Ave. Gran Bretaña 1111, Playa Ancha, Casilla 5030, Valparaíso, Chile

the best known Oosterhoff type II globular cluster. Yet, M62 is more metal-rich by about 1 dex, with an $[\text{Fe}/\text{H}] = -1.29$, compared with $[\text{Fe}/\text{H}] = -2.26$ for M15 (Harris 1996). Since there is significant debate as to whether metallicity or HB morphology play the dominant role in defining the Oosterhoff types of globular clusters (e.g., Clement 2000; Pritzl et al. 2002), M62 can provide a very important constraint on whether metallicity differences, at a fixed HB morphology, can by themselves change the classification of an object from Oosterhoff type II (as in the case of M15) to Oosterhoff type I (as is typical of globular clusters with metallicity similar to M62's, but with significantly redder HB types).

The main time-series study of M62 available in the literature so far was carried out by van Agt & Oosterhoff (1959), where extensive photographic observations were presented, and periods derived for a total of 74 (out of 83) stars. More recently, Malakhova et al. (1997) provided a list of 43 additional RR Lyrae star candidates in the cluster, but without determining their periods nor their detailed variability status. As a consequence, 126 variable star candidates have been listed for the cluster, 74 of which have known periods of variability (Clement et al. 2001, and references therein).

Given the availability of high-quality CCD observations

and state-of-the-art image subtraction techniques, we expected to find many new variable stars in the course of our new time-series study of M62. Indeed, we were able to find more than 200 RR Lyrae stars in M62, in addition to a large number of long-period variables (LPV's) and type II Cepheids (CpII).

As reported in Contreras et al. (2005), the newly detected RR Lyrae stars in M62 offer us important insight into the role played by metallicity in defining Oosterhoff type, suggesting that M62 is indeed an Oosterhoff type I (OoI) object, in spite of its predominantly blue HB morphology, but in accord with its fairly high metallicity.

The main purpose of the present paper is to provide the new, extensive variability data for M62, upon which the preliminary results by Contreras et al. (2005) were based. We begin in §2 by describing our data and reduction procedures. In §3 we discuss how the variable stars were detected in our data. In §4 we describe the results of a Fourier decomposition analysis of the measured light curves. A CMD is produced in §5, where our approach to account for the effects of differential reddening is also described. In §6 we revisit the Oosterhoff type determination for the cluster. In §7 we apply the “A-method” to study the He abundance in the cluster, and in §8 we provide a summary of our results.

Table 1
Photometric Parameters for M62 Variables

| ID | RA (J2000) | DEC (J2000) | P (d) | A_B | A_V | $\langle B \rangle$ | $\langle V \rangle$ | $(B-V)_{\text{mag}}$ | $E(B-V)$ | Type |
|-----|------------|-------------|---------|-------|-------|---------------------|---------------------|----------------------|----------|------|
| V1 | 255.317419 | -30.113051 | 0.5047 | ... | ... | ... | ... | ... | ... | RRab |
| V2 | 255.295900 | -30.134135 | 10.59 | 1.164 | 1.054 | 14.408 | 13.418 | 1.036 | ... | CpII |
| V3 | 255.275491 | -30.116931 | 0.4913 | ... | ... | ... | ... | ... | ... | RRab |
| V4 | 255.273855 | -30.126022 | 0.54113 | 1.382 | 1.068 | 16.889 | 16.109 | 0.820 | 0.511 | RRab |
| V6 | 255.277571 | -30.105578 | 0.4920 | 1.363 | 1.082 | 16.861 | 16.121 | 0.772 | 0.442 | RRab |
| V7 | 255.310374 | -30.068129 | 0.5640 | 1.235 | 0.946 | 16.799 | 16.044 | 0.785 | 0.462 | RRab |
| V8 | 255.273122 | -30.070173 | 0.5327 | 1.315 | 1.009 | 16.779 | 16.034 | 0.780 | 0.462 | RRab |
| V10 | 255.157448 | -30.071484 | 0.53259 | 1.531 | 1.208 | 16.616 | 15.948 | 0.710 | 0.387 | RRab |
| V11 | 255.156348 | -30.080112 | 0.59823 | 0.994 | 0.749 | 16.651 | 15.921 | 0.746 | 0.369 | RRab |
| V13 | 255.302296 | -30.105842 | 0.3033 | ... | ... | ... | ... | ... | ... | RRc |
| V16 | 255.279503 | -30.088975 | 0.594 | 1.441 | 1.105 | 16.620 | 15.883 | 0.774 | 0.434 | RRab |
| V17 | 255.296272 | -30.086534 | 0.529 | 1.475 | 1.135 | 16.873 | 16.109 | 0.803 | 0.480 | RRab |
| V18 | 255.292820 | -30.089474 | 0.5241 | 1.285 | 1.027 | 16.937 | 16.156 | 0.806 | 0.461 | RRab |
| V19 | 255.298855 | -30.096809 | 0.5227 | ... | ... | ... | ... | ... | ... | RRab |
| V20 | 255.345754 | -30.070601 | 0.47201 | 1.590 | 1.252 | 16.842 | 16.099 | 0.792 | 0.499 | RRab |
| V21 | 255.337973 | -30.092659 | 0.4502 | 1.651 | 1.301 | 16.990 | 16.267 | 0.781 | 0.497 | RRab |
| V22 | 255.324073 | -30.111547 | 0.5013 | ... | ... | ... | ... | ... | ... | RRab |
| V23 | 255.280529 | -30.125258 | 0.44821 | 0.693 | 0.306 | 16.011 | 14.699 | 1.329 | ... | RRab |
| V24 | 255.323323 | -30.125505 | 0.5223 | 1.480 | 1.121 | 17.309 | 16.422 | 0.932 | 0.620 | RRab |
| V25 | 255.353541 | -30.134815 | 0.4459 | 1.691 | 1.292 | 17.463 | 16.626 | 0.890 | 0.596 | RRab |
| V26 | 255.245931 | -30.198522 | 0.3717 | 1.680 | 1.210 | 14.343 | 13.547 | 0.862 | 0.607 | RRab |
| V27 | 255.302024 | -30.131513 | 0.44916 | 1.703 | 1.382 | 17.183 | 16.361 | 0.869 | 0.562 | RRab |
| V28 | 255.353523 | -30.109435 | 0.4978 | 1.424 | 1.123 | 17.348 | 16.610 | 0.774 | ... | RRab |
| V29 | 255.353458 | -30.110630 | 0.5653 | 1.551 | 1.184 | 17.238 | 16.396 | 0.888 | 0.574 | RRab |
| V30 | 255.285077 | -30.165287 | 0.3041 | 0.565 | 0.422 | 17.308 | 16.502 | 0.813 | ... | RRc |
| V31 | 255.289800 | -30.154549 | 0.4855 | 1.577 | 1.271 | 17.496 | 16.590 | 0.954 | 0.655 | RRab |
| V32 | 255.304371 | -30.152469 | 0.5479 | 1.315 | 0.953 | 17.499 | 16.571 | 0.966 | 0.688 | RRab |
| V33 | 255.300167 | -30.147727 | 0.5736 | 1.273 | 0.973 | 17.600 | 16.620 | 1.009 | 0.688 | RRab |
| V34 | 255.284474 | -30.116560 | 0.5834 | 1.402 | 1.053 | 16.789 | 15.955 | 0.876 | 0.559 | RRab |
| V35 | 255.267377 | -30.108630 | 0.5292 | 1.271 | 0.975 | 16.942 | 16.153 | 0.822 | 0.499 | RRab |
| V36 | 255.290154 | -30.080264 | 0.6527 | 0.819 | 0.659 | 16.730 | 15.933 | 0.810 | 0.442 | RRab |
| V37 | 255.286882 | -30.113188 | 0.5844 | ... | ... | ... | ... | ... | ... | RRab |
| V38 | 255.297099 | -30.127381 | 0.77083 | ... | ... | ... | ... | ... | ... | RRab |
| V39 | 255.264623 | -30.098901 | 0.6401 | 0.607 | 0.479 | 16.897 | 16.065 | 0.840 | 0.470 | RRab |
| V40 | 255.264299 | -30.102617 | 0.3012 | 0.622 | 0.531 | 16.790 | 16.124 | 0.673 | ... | RRc |
| V41 | 255.265477 | -30.103925 | 0.5590 | 1.078 | 0.801 | 16.909 | 16.112 | 0.821 | 0.482 | RRab |
| V42 | 255.261784 | -30.101339 | 0.2469 | 0.434 | 0.351 | 16.689 | 16.085 | 0.608 | ... | RRc |
| V43 | 255.285001 | -30.171389 | 0.56356 | 1.159 | 0.859 | 17.377 | 16.481 | 0.925 | 0.832 | RRab |
| V44 | 255.289436 | -30.148943 | 0.4456 | 1.471 | 1.122 | 17.631 | 16.724 | 0.954 | 0.681 | RRab |
| V45 | 255.324166 | -30.166686 | 0.51688 | ... | ... | ... | ... | ... | ... | RRab |
| V48 | 255.276867 | -30.151301 | 0.7432 | 0.934 | 0.725 | 17.108 | 16.185 | 0.940 | 0.571 | RRab |
| V49 | 255.349296 | -30.143648 | 0.5434 | 1.239 | 0.962 | 17.414 | 16.524 | 0.918 | 0.599 | RRab |
| V50 | 255.394967 | -30.123945 | 0.50264 | ... | ... | ... | ... | ... | ... | RRab |
| V51 | 255.398036 | -30.060953 | 0.2618 | 0.617 | ... | 16.883 | ... | ... | ... | RRc |

Table 1 — *Continued*

| ID | RA (J2000) | DEC (J2000) | P (d) | A_B | A_V | $\langle B \rangle$ | $\langle V \rangle$ | $(B-V)_{\text{mag}}$ | $E(B-V)$ | Type |
|-------|------------|-------------|---------|-------|-------|---------------------|---------------------|----------------------|----------|------|
| V52 | 255.328949 | -30.165131 | 0.50538 | ... | ... | ... | ... | ... | ... | RRab |
| V53 | 255.268551 | -30.143154 | 0.2731 | 0.654 | 0.502 | 17.296 | 16.512 | 0.794 | ... | RRc |
| V56 | 255.315460 | -30.081934 | 0.5616 | 1.164 | 0.857 | 17.089 | 16.249 | 0.864 | 0.520 | RRab |
| V57 | 255.319997 | -30.081330 | 0.5564 | 1.096 | 0.854 | 17.074 | 16.235 | 0.864 | 0.535 | RRab |
| V58 | 255.272245 | -30.106241 | 0.481 | 1.159 | 0.996 | 16.832 | ... | ... | ... | RRab |
| V59 | 255.343055 | -30.088719 | 0.5791 | 1.148 | 0.871 | 17.093 | 16.250 | 0.870 | 0.550 | RRab |
| V61 | 255.372598 | -30.061961 | 0.2660 | 0.655 | ... | 17.095 | ... | ... | ... | RRc |
| V62 | 255.380443 | -30.085530 | 0.54807 | 1.235 | 0.958 | 17.048 | 16.230 | 0.845 | 0.519 | RRab |
| V63 | 255.338601 | -30.143041 | 0.6421 | 0.831 | 0.612 | 17.533 | 16.547 | 1.001 | 0.642 | RRab |
| V64 | 255.361610 | -30.195524 | 0.47299 | 0.785 | 0.592 | 17.077 | 16.157 | 0.937 | 0.614 | RRab |
| V65 | 255.275462 | -30.077039 | 0.2523 | 0.485 | 0.397 | 16.705 | 16.086 | 0.623 | ... | RRc |
| V66 | 255.201993 | -30.110297 | 0.33383 | 0.570 | 0.420 | 16.676 | 16.011 | 0.674 | ... | RRc |
| V69 | 255.343090 | -30.084393 | 0.3136 | 0.556 | 0.417 | 16.996 | 16.249 | 0.754 | ... | RRc |
| V72 | 255.245694 | -30.144019 | 0.468 | 1.422 | 1.053 | 17.034 | 16.286 | 0.795 | 0.529 | RRab |
| V73 | 255.238968 | -30.144283 | 1.70 | 1.036 | 0.788 | 16.147 | 15.243 | 0.923 | ... | CpII |
| V74 | 255.297471 | -30.129784 | 0.4667 | ... | ... | ... | ... | ... | ... | RRab |
| V77 | 255.392629 | -30.105263 | 0.319 | 0.531 | 0.405 | 17.240 | 16.427 | 0.820 | ... | RRc |
| V78 | 255.412564 | -30.066713 | 0.62170 | 0.880 | 0.613 | 17.326 | 16.362 | 0.979 | 0.619 | RRab |
| V80 | 255.276084 | -30.089919 | 0.5962 | 0.914 | 0.645 | 16.985 | 16.090 | 0.911 | 0.739 | RRab |
| V81 | 255.267912 | -30.088047 | 0.5309 | 1.325 | 1.042 | 16.821 | 16.078 | 0.774 | 0.449 | RRab |
| V82 | 255.291579 | -30.133857 | 0.5648 | 0.835 | 0.642 | 17.291 | 16.479 | 0.826 | 0.483 | RRab |
| V83 | 255.309339 | -30.120442 | 0.4676 | ... | ... | ... | ... | ... | ... | RRab |
| NV84 | 255.271467 | -30.134929 | 0.7312 | 0.636 | 0.461 | 17.003 | 16.111 | 0.900 | 0.523 | RRab |
| NV85 | 255.276401 | -30.139297 | 0.3196 | 0.484 | 0.432 | 17.189 | 16.365 | 0.826 | ... | RRc |
| NV86 | 255.282427 | -30.095331 | 0.2913 | 0.565 | 0.433 | 16.795 | 16.112 | 0.690 | ... | RRc |
| NV87 | 255.284966 | -30.088009 | 0.6424 | 0.401 | 0.296 | 16.876 | 16.049 | 0.830 | 0.449 | RRab |
| NV88 | 255.285771 | -30.091009 | 0.5807 | 0.922 | 0.737 | 16.924 | 16.129 | 0.810 | 0.437 | RRab |
| NV89 | 255.288146 | -30.130509 | 0.5581 | ... | ... | ... | ... | ... | ... | RRab |
| NV90 | 255.290712 | -30.138332 | 0.3273 | 0.602 | 0.462 | 17.391 | 16.534 | 0.865 | ... | RRc |
| NV91 | 255.293574 | -30.132221 | 0.3167 | 0.521 | 0.421 | 17.090 | 16.337 | 0.758 | ... | RRc |
| NV92 | 255.294328 | -30.135833 | 0.5256 | ... | ... | ... | ... | ... | ... | RRab |
| NV93 | 255.298447 | -30.097374 | 0.552 | 1.205 | 0.966 | 17.249 | 16.340 | 0.935 | 0.600 | RRab |
| NV94 | 255.306828 | -30.090652 | 0.3181 | ... | ... | ... | ... | ... | ... | RRc |
| NV95 | 255.311633 | -30.142402 | 0.4941 | 1.618 | 1.226 | 17.533 | 16.609 | 0.970 | 0.668 | RRab |
| NV96 | 255.315438 | -30.140551 | 0.4663 | 1.582 | 1.257 | 17.452 | 16.615 | 0.880 | 0.572 | RRab |
| NV97 | 255.323047 | -30.096211 | 0.5510 | 1.166 | 0.883 | 17.096 | 16.262 | 0.861 | 0.534 | RRab |
| NV98 | 255.321234 | -30.147140 | 0.5620 | 1.113 | 0.878 | 17.611 | 16.670 | 0.969 | 0.645 | RRab |
| NV99 | 255.323772 | -30.144410 | 0.6028 | 0.565 | 0.410 | 17.661 | 16.644 | 1.023 | 0.653 | RRab |
| NV100 | 255.332677 | -30.100980 | 0.2665 | 0.612 | 0.490 | 17.097 | 16.370 | 0.735 | ... | RRc |
| NV101 | 255.331020 | -30.146758 | 0.3055 | 0.493 | 0.397 | 17.333 | 16.516 | 0.821 | ... | RRc |
| NV102 | 255.334042 | -30.094895 | 0.6307 | 0.737 | 0.541 | 17.048 | 16.174 | 0.885 | 0.523 | RRab |
| NV103 | 255.331861 | -30.150089 | 0.4836 | 0.825 | 0.611 | 17.588 | 16.655 | 0.949 | 0.602 | RRab |
| NV104 | 255.335589 | -30.111854 | 0.6307 | 0.306 | 0.221 | 17.290 | 16.380 | 0.913 | ... | RRc? |
| NV105 | 255.337117 | -30.101376 | 0.5205 | 1.517 | 1.162 | 17.181 | 16.351 | 0.871 | 0.565 | RRab |
| NV106 | 255.342344 | -30.102395 | 0.5037 | 1.504 | 1.153 | 17.175 | 16.359 | 0.857 | 0.549 | RRab |
| NV107 | 255.342654 | -30.121002 | 0.5728 | 0.898 | 0.680 | 17.472 | 16.541 | 0.947 | 0.593 | RRab |
| NV108 | 255.343116 | -30.112112 | 0.2988 | 0.539 | 0.442 | 17.238 | 16.468 | 0.774 | ... | RRc |
| NV109 | 255.348015 | -30.124260 | 0.6078 | 1.015 | 0.700 | 17.464 | 16.525 | 0.959 | 0.602 | RRab |
| NV110 | 255.353263 | -30.116493 | 0.3354 | 0.584 | 0.417 | 17.320 | 16.483 | 0.844 | ... | RRc |
| NV111 | 255.264451 | -30.188755 | 0.2494 | 0.462 | 0.311 | 17.012 | 16.317 | 0.701 | ... | RRc |
| NV112 | 255.191976 | -30.186995 | 0.503 | ... | ... | ... | ... | ... | ... | RRab |
| NV113 | 255.323088 | -30.186512 | 0.478 | 1.632 | 1.221 | 17.226 | 16.404 | 0.873 | 0.578 | RRab |
| NV114 | 255.427287 | -30.178179 | 0.398 | 1.063 | 1.010 | 18.423 | 17.135 | 1.294 | ... | EB |
| NV115 | 255.349885 | -30.176159 | 0.2690 | 0.671 | 0.519 | 17.276 | 16.529 | 0.757 | ... | RRc |
| NV116 | 255.356841 | -30.175140 | 0.615 | 0.558 | 0.390 | 17.290 | 16.384 | 0.913 | 0.551 | RRab |
| NV117 | 255.247513 | -30.170192 | 0.321 | 0.236 | ... | 17.246 | ... | ... | ... | RRc |
| NV118 | 255.353800 | -30.166045 | 0.2987 | 0.558 | 0.455 | 17.221 | 16.468 | 0.760 | ... | RRc |
| NV119 | 255.312109 | -30.163121 | 0.3191 | 0.525 | 0.397 | 17.552 | 16.678 | 0.880 | ... | RRc |
| NV120 | 255.413338 | -30.160585 | 0.489 | 1.658 | 1.271 | ... | ... | ... | ... | RRab |
| NV121 | 255.299162 | -30.159912 | 0.2805 | 0.498 | 0.378 | 18.060 | 17.251 | 0.814 | ... | RRc |
| NV122 | 255.222519 | -30.139789 | 0.373 | 0.116 | ... | 16.845 | ... | ... | ... | RRc |
| NV123 | 255.222694 | -30.138895 | 0.3043 | 0.535 | 0.439 | 16.990 | 16.262 | 0.733 | ... | RRc |
| NV124 | 255.287656 | -30.127940 | 0.4855 | 1.539 | 1.115 | 16.817 | ... | ... | ... | RRab |
| NV125 | 255.292043 | -30.127814 | 0.2737 | ... | ... | ... | ... | ... | ... | RRc |
| NV126 | 255.310969 | -30.127268 | 0.5133 | ... | ... | ... | ... | ... | ... | RRab |
| NV127 | 255.288948 | -30.127077 | 0.5328 | 1.677 | 1.307 | 16.676 | 15.942 | 0.792 | 0.502 | RRab |
| NV128 | 255.328694 | -30.127022 | 0.2504 | 0.538 | 0.359 | 17.519 | 16.692 | 0.836 | ... | RRc |
| NV129 | 255.311556 | -30.126846 | 0.3292 | ... | ... | ... | ... | ... | ... | RRc |
| NV130 | 255.299567 | -30.125709 | 0.2613 | ... | ... | ... | ... | ... | ... | RRc |
| NV131 | 255.327951 | -30.125428 | 0.3132 | 0.538 | 0.431 | 17.371 | 16.530 | 0.848 | ... | RRc |
| NV132 | 255.300206 | -30.124985 | 0.2842 | 0.764 | 0.628 | 16.919 | 16.189 | 0.741 | ... | RRc |
| NV133 | 255.303920 | -30.124868 | 0.3156 | 0.565 | 0.479 | 16.988 | 16.190 | 0.802 | ... | RRc |
| NV134 | 255.304938 | -30.124915 | 0.336 | ... | ... | ... | ... | ... | ... | RRc |
| NV135 | 255.212612 | -30.124641 | 0.593 | 0.924 | 0.698 | 17.099 | 16.263 | 0.853 | 0.504 | RRab |
| NV136 | 255.313600 | -30.124235 | 0.6258 | 1.160 | 0.878 | 17.105 | 16.227 | 0.904 | 0.553 | RRab |
| NV137 | 255.300694 | -30.123833 | 0.515 | ... | ... | ... | ... | ... | ... | RRab |
| NV138 | 255.303221 | -30.123809 | 0.6051 | ... | ... | ... | ... | ... | ... | RRab |

Table 1 — *Continued*

| ID | RA (J2000) | DEC (J2000) | P (d) | A_B | A_V | $\langle B \rangle$ | $\langle V \rangle$ | $(B-V)_{\text{mag}}$ | $E(B-V)$ | Type |
|-------|------------|-------------|---------|-------|-------|---------------------|---------------------|----------------------|----------|-------|
| NV139 | 255.304235 | -30.123830 | 0.5405 | ... | ... | ... | ... | ... | ... | RRab |
| NV140 | 255.313693 | -30.123622 | 0.3830 | 0.541 | 0.427 | 16.905 | 16.097 | 0.813 | ... | RRc |
| NV141 | 255.302897 | -30.123377 | 0.2994 | ... | ... | ... | ... | ... | ... | RRc |
| NV142 | 255.324870 | -30.122729 | 0.2758 | ... | ... | ... | ... | ... | ... | RRc |
| NV143 | 255.299682 | -30.121951 | 0.2959 | ... | ... | ... | ... | ... | ... | RRc |
| NV144 | 255.297520 | -30.121835 | 0.6105 | ... | ... | ... | ... | ... | ... | RRab |
| NV145 | 255.310817 | -30.121214 | 0.5665 | ... | ... | ... | ... | ... | ... | RRab |
| NV146 | 255.296802 | -30.121044 | 0.4660 | ... | ... | ... | ... | ... | ... | RRab |
| NV147 | 255.301092 | -30.120878 | 0.3259 | ... | ... | ... | ... | ... | ... | RRc |
| NV148 | 255.307127 | -30.120699 | 0.5606 | ... | ... | ... | ... | ... | ... | RRab |
| NV149 | 255.300972 | -30.120147 | 0.319 | ... | ... | ... | ... | ... | ... | RRc |
| NV150 | 255.290041 | -30.119827 | 0.5480 | 0.910 | 0.686 | 17.001 | 16.159 | 0.862 | 0.538 | RRab |
| NV151 | 255.294859 | -30.119358 | 0.3153 | ... | ... | ... | ... | ... | ... | RRc |
| NV152 | 255.321269 | -30.119151 | 0.3032 | ... | ... | ... | ... | ... | ... | RRc |
| NV153 | 255.266009 | -30.118983 | 0.3129 | 0.596 | 0.462 | 16.807 | 16.109 | 0.706 | ... | RRc |
| NV154 | 255.290525 | -30.118882 | 0.3151 | ... | ... | ... | ... | ... | ... | RRc |
| NV155 | 255.304738 | -30.118780 | 0.271 | ... | ... | ... | ... | ... | ... | RRc |
| NV156 | 255.301102 | -30.118553 | 0.577 | ... | ... | ... | ... | ... | ... | RRab |
| NV157 | 255.307981 | -30.118448 | 0.7195 | ... | ... | ... | ... | ... | ... | RRab |
| NV158 | 255.300638 | -30.118371 | 0.264 | ... | ... | ... | ... | ... | ... | RRc |
| NV159 | 255.289372 | -30.118087 | 0.3763 | ... | ... | ... | ... | ... | ... | RRc |
| NV160 | 255.292290 | -30.118020 | 0.5437 | 1.482 | 1.218 | 16.933 | 16.147 | 0.819 | 0.487 | RRab |
| NV161 | 255.310399 | -30.117484 | 0.5568 | ... | ... | ... | ... | ... | ... | RRab |
| NV162 | 255.304420 | -30.117429 | 0.6032 | ... | ... | ... | ... | ... | ... | RRab |
| NV163 | 255.306762 | -30.117204 | 0.5943 | ... | ... | ... | ... | ... | ... | RRab |
| NV164 | 255.303820 | -30.116505 | 7.6 | ... | ... | ... | ... | ... | ... | CpII |
| NV165 | 255.302432 | -30.116402 | 0.4520 | ... | ... | ... | ... | ... | ... | RRab |
| NV166 | 255.304920 | -30.116240 | 0.290 | ... | ... | ... | ... | ... | ... | RRc |
| NV167 | 255.314500 | -30.116126 | 0.630 | ... | ... | ... | ... | ... | ... | RRab |
| NV168 | 255.270280 | -30.115961 | 0.5754 | 0.538 | 0.417 | 16.965 | 16.143 | 0.827 | 0.489 | RRab |
| NV169 | 255.291652 | -30.115633 | 0.5144 | ... | ... | ... | ... | ... | ... | RRab |
| NV170 | 255.306553 | -30.115631 | 0.635 | ... | ... | ... | ... | ... | ... | ? |
| NV171 | 255.318789 | -30.115528 | 0.6482 | 0.322 | 0.254 | 17.159 | 16.246 | 0.914 | ... | RRc? |
| NV172 | 255.308393 | -30.115490 | 0.3132 | ... | ... | ... | ... | ... | ... | RRc |
| NV173 | 255.305549 | -30.115363 | 0.347 | ... | ... | ... | ... | ... | ... | RRc |
| NV174 | 255.301761 | -30.115313 | 0.3175 | ... | ... | ... | ... | ... | ... | RRc |
| NV175 | 255.321256 | -30.115305 | 0.2816 | 0.643 | 0.516 | 17.08 | 16.372 | 0.725 | ... | RRc |
| NV176 | 255.305474 | -30.114681 | 0.2628 | ... | ... | ... | ... | ... | ... | RRc |
| NV177 | 255.291754 | -30.114502 | 0.6851 | ... | ... | ... | ... | ... | ... | RRab |
| NV178 | 255.304743 | -30.114507 | 0.407 | ... | ... | ... | ... | ... | ... | RRc |
| NV179 | 255.301488 | -30.114427 | 0.5483 | ... | ... | ... | ... | ... | ... | RRab |
| NV180 | 255.296731 | -30.114401 | 1.376 | ... | ... | ... | ... | ... | ... | CpII |
| NV181 | 255.295084 | -30.113733 | 0.5895 | ... | ... | ... | ... | ... | ... | RRab |
| NV182 | 255.300463 | -30.113602 | 0.505 | ... | ... | ... | ... | ... | ... | RRab |
| NV183 | 255.305893 | -30.113635 | 0.5686 | ... | ... | ... | ... | ... | ... | RRab |
| NV184 | 255.302188 | -30.113549 | 0.5722 | ... | ... | ... | ... | ... | ... | RRab |
| NV185 | 255.313926 | -30.113517 | 0.591 | ... | ... | ... | ... | ... | ... | RRab |
| NV186 | 255.307716 | -30.113428 | 0.3025 | ... | ... | ... | ... | ... | ... | RRc |
| NV187 | 255.298718 | -30.113290 | 0.491 | ... | ... | ... | ... | ... | ... | RRab |
| NV188 | 255.303150 | -30.113177 | 0.436 | ... | ... | ... | ... | ... | ... | RRab |
| NV189 | 255.315829 | -30.113097 | 0.5617 | ... | ... | ... | ... | ... | ... | RRab |
| NV190 | 255.302756 | -30.112618 | 0.554 | ... | ... | ... | ... | ... | ... | RRab |
| NV191 | 255.305548 | -30.112558 | 0.5857 | ... | ... | ... | ... | ... | ... | RRab |
| NV192 | 255.353057 | -30.112569 | 0.2652 | 0.406 | 0.314 | 17.250 | 16.510 | 0.743 | ... | RRc |
| NV193 | 255.314500 | -30.112496 | 0.3198 | ... | ... | ... | ... | ... | ... | RRc |
| NV194 | 255.317154 | -30.112403 | 0.505 | ... | ... | ... | ... | ... | ... | RRab |
| NV195 | 255.298155 | -30.112409 | 0.47 | ... | ... | ... | ... | ... | ... | RRc |
| NV196 | 255.288121 | -30.112265 | 0.3109 | ... | ... | ... | ... | ... | ... | RRc |
| NV197 | 255.304747 | -30.111837 | 0.3183 | ... | ... | ... | ... | ... | ... | RRc |
| NV198 | 255.289817 | -30.111245 | 0.5763 | 1.102 | 0.782 | 16.922 | 16.059 | 0.889 | 0.559 | RRab |
| NV199 | 255.315134 | -30.110762 | 0.5568 | ... | ... | ... | ... | ... | ... | RRab |
| NV200 | 255.293965 | -30.110272 | 0.487 | ... | ... | ... | ... | ... | ... | RRab |
| NV201 | 255.314913 | -30.108397 | 0.2507 | ... | ... | ... | ... | ... | ... | RRc |
| NV202 | 255.307417 | -30.108318 | 0.2709 | 0.517 | 0.439 | 16.974 | 16.258 | 0.720 | ... | RRc |
| NV203 | 255.301002 | -30.108253 | 0.491 | ... | ... | ... | ... | ... | ... | RRab |
| NV204 | 255.284814 | -30.108090 | 0.263 | 0.415 | 0.329 | 16.922 | 16.224 | 0.701 | ... | RRc |
| NV205 | 255.295998 | -30.107995 | 0.552 | ... | ... | ... | ... | ... | ... | RRab |
| NV206 | 255.300336 | -30.107351 | 0.640 | ... | ... | ... | ... | ... | ... | RRab |
| NV207 | 255.299857 | -30.106901 | 0.265 | ... | ... | ... | ... | ... | ... | RRc |
| NV208 | 255.298778 | -30.106808 | 0.5410 | ... | ... | ... | ... | ... | ... | RRab |
| NV209 | 255.307591 | -30.106368 | 0.2883 | ... | ... | ... | ... | ... | ... | RRc |
| NV210 | 255.309869 | -30.106245 | 0.4370 | 1.902 | 1.647 | 17.015 | 16.207 | 0.861 | 0.553 | RRab |
| NV211 | 255.319518 | -30.106219 | 0.3327 | ... | ... | ... | ... | ... | ... | RRc |
| NV212 | 255.314221 | -30.105641 | 0.6072 | ... | ... | ... | ... | ... | ... | RRab |
| NV213 | 255.303032 | -30.104438 | 0.5853 | ... | ... | ... | ... | ... | ... | RRab |
| NV214 | 255.318374 | -30.103102 | 0.587 | 1.004 | 0.776 | 17.154 | 16.299 | 0.875 | 0.538 | RRab |
| NV215 | 255.305126 | -30.102857 | 0.4616 | ... | ... | ... | ... | ... | ... | RRab? |

Table 1 — *Continued*

| ID | RA (J2000) | DEC (J2000) | P (d) | A_B | A_V | $\langle B \rangle$ | $\langle V \rangle$ | $(B-V)_{\text{mag}}$ | $E(B-V)$ | Type |
|-------|------------|-------------|---------|-------|-------|---------------------|---------------------|----------------------|----------|----------|
| NV216 | 255.298332 | -30.102701 | 0.2666 | ... | ... | ... | ... | ... | ... | RRc |
| NV217 | 255.283447 | -30.102377 | 0.3203 | ... | ... | ... | ... | ... | ... | RRc |
| NV218 | 255.307103 | -30.101639 | 0.4447 | 1.485 | 1.249 | 16.867 | 16.095 | 0.804 | 0.492 | RRab |
| NV219 | 255.290591 | -30.101456 | 0.7177 | 0.862 | 0.744 | 16.940 | 16.032 | 0.916 | 0.509 | RRab |
| NV220 | 255.303126 | -30.101010 | 0.496 | ... | ... | ... | ... | ... | ... | RRab |
| NV221 | 255.265266 | -30.091025 | 0.3300 | 0.555 | 0.425 | 16.802 | 16.085 | 0.725 | ... | RRc |
| NV222 | 255.250721 | -30.080969 | 0.460 | ... | ... | ... | ... | ... | ... | RRab |
| NV223 | 255.323255 | -30.080828 | 0.5325 | 1.346 | 1.026 | 17.123 | 16.305 | 0.852 | 0.529 | RRab |
| NV224 | 255.395528 | -30.079961 | 0.3196 | 0.546 | 0.417 | 17.725 | 16.952 | 0.779 | ... | RRc |
| NV225 | 255.322496 | -30.079209 | 0.2884 | 0.396 | 0.252 | 16.352 | 15.353 | 1.004 | ... | RRc |
| NV226 | 255.285658 | -30.071786 | 0.6301 | 1.073 | 0.796 | 16.736 | 15.984 | 0.776 | 0.450 | RRab |
| NV227 | 255.450562 | -30.068877 | 0.456 | 1.725 | 1.290 | 18.629 | 17.774 | 0.899 | 0.564 | RRab |
| NV228 | 255.334192 | -30.068270 | 0.6417 | 0.380 | 0.322 | 17.132 | 16.253 | 0.881 | 0.479 | RRab |
| NV229 | 255.337618 | -30.066281 | 0.2773 | 0.295 | 0.248 | 16.765 | 16.106 | 0.660 | ... | RRc |
| NV230 | 255.332977 | -30.096293 | | ... | ... | ... | ... | ... | ... | LP |
| NV231 | 255.324541 | -30.097949 | ~16 | ... | ... | ... | ... | ... | ... | LP/CpII? |
| NV232 | 255.321150 | -30.136159 | | ... | ... | ... | ... | ... | ... | LP |
| NV233 | 255.318726 | -30.108153 | ~49 | ... | ... | ... | ... | ... | ... | LP |
| NV234 | 255.308946 | -30.113105 | | ... | ... | ... | ... | ... | ... | LP |
| NV235 | 255.307303 | -30.111160 | | ... | ... | ... | ... | ... | ... | LP |
| NV236 | 255.307158 | -30.110023 | ~50 | ... | ... | ... | ... | ... | ... | LP |
| NV237 | 255.303834 | -30.130456 | | ... | ... | ... | ... | ... | ... | LP |
| NV238 | 255.304566 | -30.106671 | | ... | ... | ... | ... | ... | ... | LP |
| NV239 | 255.303782 | -30.113794 | ~75 | ... | ... | ... | ... | ... | ... | LP |
| NV240 | 255.303710 | -30.118210 | | ... | ... | ... | ... | ... | ... | LP |
| NV241 | 255.303521 | -30.116544 | 0.525 | ... | ... | ... | ... | ... | ... | RRab? |
| NV242 | 255.302059 | -30.108011 | ~36 | ... | ... | ... | ... | ... | ... | LP |
| NV243 | 255.301054 | -30.113012 | 0.4911 | ... | ... | ... | ... | ... | ... | RRab |
| NV244 | 255.298619 | -30.119052 | | ... | ... | ... | ... | ... | ... | LP |
| NV245 | 255.297277 | -30.084141 | ~88 | ... | ... | ... | ... | ... | ... | LP |
| NV246 | 255.295958 | -30.105957 | 0.5086 | ... | ... | ... | ... | ... | ... | RRab |
| NV247 | 255.295155 | -30.120411 | 0.4928 | ... | ... | ... | ... | ... | ... | RRab |
| NV248 | 255.294099 | -30.114300 | | ... | ... | ... | ... | ... | ... | LP |
| NV249 | 255.292809 | -30.111699 | 0.2476 | ... | ... | ... | ... | ... | ... | RRc |
| NV250 | 255.292034 | -30.119580 | ~65 | ... | ... | ... | ... | ... | ... | LP |
| NV251 | 255.290391 | -30.115419 | | ... | ... | ... | ... | ... | ... | LP |
| NV252 | 255.281460 | -30.119274 | | ... | ... | ... | ... | ... | ... | LP |
| NV253 | 255.280065 | -30.102644 | | ... | ... | ... | ... | ... | ... | LP |
| NV254 | 255.278510 | -30.126721 | ~90 | ... | ... | ... | ... | ... | ... | LP |
| NV255 | 255.278235 | -30.114604 | | ... | ... | ... | ... | ... | ... | LP |
| NV256 | 255.278240 | -30.102156 | | ... | ... | ... | ... | ... | ... | LP |
| NV257 | 255.274444 | -30.135636 | ~33 | ... | ... | ... | ... | ... | ... | LP |
| NV258 | 255.308126 | -30.120434 | | ... | ... | ... | ... | ... | ... | LP |
| NV259 | 255.298877 | -30.063971 | 0.6704 | ... | ... | ... | ... | ... | ... | RRab? |
| NV260 | 255.305121 | -30.102731 | 0.2540 | ... | ... | ... | ... | ... | ... | RRc |
| NV261 | 255.300681 | -30.123291 | 0.5041 | ... | ... | ... | ... | ... | ... | RRab |
| NV262 | 255.261271 | -30.109493 | | ... | ... | ... | ... | ... | ... | LP |

2. OBSERVATIONS AND DATA REDUCTIONS

M62 was observed in conjunction with M69 (NGC 6637; Escobar et al. 2010, in preparation) and NGC 5286 (Zorotovic et al. 2009, 2010) as part of a long-term project aimed at completing the census of (bright) variable stars in Galactic globular clusters (Catelan et al. 2006). Time-series observations in B and V were obtained with the Warsaw 1.3m telescope at the Las Campanas Observatory (LCO), in the course of 7 consecutive nights over the period April 6–13 2003. The camera used is the 8kMOSAIC camera, comprised of eight 2040×4096 chips, with a scale $0.26''/\text{pixel}$ giving an observing area equal to $35' \times 35'$. The cluster was roughly centered on chip 2, and so in this paper we focus our analysis on this chip (which covers a sky area of $8.8' \times 17.8'$). The monitored field on chip 2 covers most of the cluster area, as the tidal radius of M62 is estimated at $r = 8.95$ arcmin (Trager et al. 1995) or $r = 10.01$ arcmin (Beccari et al. 2006). The read out noise of the camera is 6 to $9 e^-$ (depending on the chip) and the gain is $6.3 e^-/\text{ADU}$. A total of 126 images in B and 126 in V were secured with this setup. During the nights of the observations, the seeing was stable enough with an average measured stellar point-spread function (PSF) on the

frames of about $0.98''$ FWHM. Exposures times ranged from 100 s to 220 s for the B frames and 30 s to 90 s for the V frames.

Observations of the standard fields PG+0918, PG+1323, PG+1525, PG+1528, PG+1633, PG+1657 and Ru 152 (Landolt 1992) were obtained on the same nights, to calibrate the data to the standard Johnson-Cousins photometric system. In order to provide better sampled light curves, the Warsaw data were complemented by observations obtained with the Cerro Tololo Inter-American Observatory (CTIO) 1.3m telescope in service mode, using the ANDICAM 1024×1024 CCD, with a scale $0.369''/\text{pixel}$, over the timespan April 24 2003 to June 30 2003. This additional dataset consists of 42 images in each of B and V , and permitted us to extend the time interval spanned by our observations up to about three months, thus resulting very useful to pin down periods and to search for long-term variability. The exposure times in this case were 145 s for the B frames and 40 s for the V frames. The seeing during these observations was on average $\sim 1.3''$, with stable and good photometric conditions. However, no standard fields were observed with the CTIO 1.3m telescope. The LCO images were pre-processed with the Warsaw 1.3m

Table 2
Photometry of the Variable Stars

| Name | Filter | JD (d) | Phase | Mag (mag) | e_Mag (mag) |
|------|--------|-----------------|--------|--------------|----------------|
| V01 | V | 2,452,736.54861 | 0.0000 | 16.2351 | 0.0031 |
| V01 | V | 2,452,736.55367 | 0.0080 | 16.2779 | 0.0042 |
| V01 | V | 2,452,736.55977 | 0.0176 | 16.2787 | 0.0051 |
| V01 | V | 2,452,736.57490 | 0.0414 | 16.3361 | 0.0054 |
| V01 | V | 2,452,736.58749 | 0.0612 | 16.3878 | 0.0059 |
| V01 | V | 2,452,736.59664 | 0.0756 | 16.3996 | 0.0059 |

Note. — This table is published in its entirety in the electronic edition of the *Astronomical Journal*. A portion is shown here for guidance regarding its form and content.

pipeline, so that no additional pre-reduction steps were necessary. The preliminary reduction of the CTIO frames, including bias subtraction and flat fielding, were carried out using the standard IRAF⁶ data reduction package.

Since no photometric calibration was obtained during the CTIO run, we used the well calibrated LCO set to link the CTIO instrumental magnitudes to the standard Johnson system. With this purpose in mind, we performed a cross correlation between the LCO and the CTIO catalogues, and then selected the best 50 stars in common that covered a sufficiently wide range in color to prevent any residual uncorrected color trend. These selected stars were then used to calibrate the CTIO data by means of a least-squares fit.

We will provide further detailed information regarding our calibration in Paper II (Contreras et al. 2010, in preparation), when a detailed analysis of our derived cluster CMD will also be provided. In any case, we note that our derived calibration equations are well defined, and have zero point errors of only about 0.006 mag in *B* and 0.011 mag in *V*, with similarly small errors in the derived color coefficients.

3. VARIABLE STARS IDENTIFICATION AND PERIOD DETERMINATION

Since the pioneering effort by Tomaney & Crofts (1996), it became clear that the image subtraction technique is one of the best tools for identifying variable stars in crowded fields like globular clusters, due to its powerful capability of comparing images after all non-variable objects have been removed. We have selected the ISIS v2.2 package for this purpose (Alard 2000). The ISIS reduction procedure that we follow consists of several steps: (1) We transform all the frames to a common coordinate grid, where the image taken with the best seeing was chosen as astrometric reference; (2) We select 10% of our frames with the best seeing conditions to construct a composite, reference photometric image; (3) We then subtract each individual frame from the composite image, after convolving the latter so that both images end up having similar PSF's. As the flux of non-variable stars on both images should be essentially identical, such objects will disappear when one image is subtracted from the other, and the remaining signal will (ideally) come exclusively from variable stars; (4) We construct a median image of all the subtracted images (known as “var.fits”) in order to enhance these weak individual (residual) signals, and thus making variable stars candidates more easily identifiable as significant peaks in the median image; (5) Finally, profile-fitting photometry was per-

⁶ IRAF is distributed by the National Optical Astronomy Observatories, which are operated by the Association of Universities for Research in Astronomy, Inc., under cooperative agreement with the National Science Foundation.

Table 3
Fourier Coefficients for RRc Variables in M62

| ID | A_{21} | A_{31} | A_{41} | ϕ_{21} | ϕ_{31} | ϕ_{41} |
|---------|----------|----------|----------|-------------|-------------------|-------------|
| V30 | 0.124 | 0.068 | 0.039 | 4.514 | 3.298 ± 0.120 | 2.196 |
| V40 | 0.144 | 0.078 | 0.057 | 4.932 | 3.624 ± 0.083 | 2.188 |
| V42 | 0.056 | 0.023 | 0.023 | 4.159 | 0.825 ± 0.448 | 0.581 |
| V53 | 0.163 | 0.096 | 0.080 | 4.761 | 2.976 ± 0.080 | 1.709 |
| V65 | 0.081 | 0.038 | 0.058 | 4.954 | 4.192 ± 0.407 | 2.908 |
| V66:: | 0.740 | 0.647 | 0.540 | 6.262 | 6.243 ± 0.009 | 6.259 |
| V69 | 0.067 | 0.057 | 0.032 | 4.673 | 3.936 ± 0.154 | 2.960 |
| V77: | 0.133 | 0.138 | 0.073 | 6.268 | 4.013 ± 0.166 | 2.574 |
| NV85 | 0.074 | 0.069 | 0.020 | 4.903 | 4.001 ± 0.120 | 1.797 |
| NV86 | 0.133 | 0.081 | 0.037 | 4.534 | 3.561 ± 0.106 | 2.417 |
| NV90: | 0.143 | 0.028 | 0.071 | 5.017 | 3.616 ± 0.455 | 2.751 |
| NV91 | 0.100 | 0.074 | 0.030 | 4.875 | 3.972 ± 0.116 | 2.817 |
| NV100 | 0.176 | 0.077 | 0.061 | 4.641 | 2.794 ± 0.089 | 1.703 |
| NV101 | 0.063 | 0.054 | 0.049 | 5.314 | 3.592 ± 0.194 | 2.700 |
| NV108 | 0.112 | 0.089 | 0.013 | 4.542 | 3.602 ± 0.115 | 2.150 |
| NV110 | 0.085 | 0.087 | 0.066 | 5.124 | 4.118 ± 0.104 | 2.866 |
| NV111:: | 0.046 | 0.086 | 0.093 | 4.375 | 4.317 ± 0.106 | 0.925 |
| NV115 | 0.184 | 0.075 | 0.052 | 4.711 | 2.807 ± 0.079 | 1.773 |
| NV118 | 0.115 | 0.074 | 0.046 | 4.633 | 3.505 ± 0.106 | 2.446 |
| NV119 | 0.090 | 0.056 | 0.043 | 4.440 | 3.793 ± 0.149 | 2.296 |
| NV121 | 0.064 | 0.083 | 0.036 | 4.642 | 3.138 ± 0.133 | 2.480 |
| NV123 | 0.101 | 0.075 | 0.041 | 4.512 | 3.839 ± 0.130 | 2.705 |
| NV128: | 0.187 | 0.025 | 0.021 | 3.889 | 1.897 ± 0.492 | 0.922 |
| NV131 | 0.095 | 0.079 | 0.039 | 5.002 | 3.764 ± 0.131 | 2.308 |
| NV132 | 0.096 | 0.042 | 0.030 | 4.058 | 4.687 ± 0.258 | 2.598 |
| NV133: | 0.115 | 0.071 | 0.050 | 4.675 | 4.236 ± 0.162 | 2.321 |
| NV140 | 0.035 | 0.079 | 0.028 | 5.767 | 4.863 ± 0.134 | 3.072 |
| NV153 | 0.113 | 0.051 | 0.037 | 4.894 | 3.688 ± 0.150 | 2.227 |
| NV175 | 0.136 | 0.101 | 0.049 | 4.558 | 3.055 ± 0.083 | 1.833 |
| NV192 | 0.090 | 0.028 | 0.026 | 4.788 | 2.338 ± 0.398 | 1.210 |
| NV202 | 0.131 | 0.046 | 0.037 | 4.878 | 2.782 ± 0.413 | 0.751 |
| NV204: | 0.176 | 0.084 | 0.081 | 4.028 | 2.769 ± 0.214 | 5.780 |
| NV221: | 0.120 | 0.110 | 0.071 | 5.602 | 4.185 ± 0.121 | 3.345 |
| NV224 | 0.109 | 0.088 | 0.036 | 4.735 | 3.653 ± 0.131 | 1.639 |
| NV225: | 0.145 | 0.091 | 0.113 | 4.341 | 4.403 ± 0.197 | 2.116 |
| NV229: | 0.060 | 0.037 | 0.005 | 4.846 | 4.208 ± 0.450 | 0.562 |

formed for each variable star candidate on the subtracted images.

Periods were determined using the phase dispersion minimization (PDM) method Stellingwerf (1978), as implemented in IRAF. PDM is a generalization of the Lafler & Kinman (1965), and essentially attempts to identify the phased light curve that produces the minimum scatter in phase. We were thus able to detect and confirm the existence of at least 245 variable stars in the field of M62, including 209 RR Lyrae, 4 type II Cepheids, 25 LPV's, 1 eclipsing binary, and 6 of uncertain nature. Among the detected RR Lyrae, 133 are fundamental-mode (RRab or RR0) pulsators, whereas 76 are first-overtone (RRc or RR1) stars. We must stress that just 1 out of the 8 Warsaw 1.3m chips were analyzed, and so the total number of (undiscovered) variable stars in the cluster is almost certainly higher. Indeed, although the Beccari et al. (2006) profile suggests that we should find $\approx 98.6\%$ of all cluster stars within $185''$ of the cluster center, we find clear evidence for an excess of variable stars whose properties are consistent with cluster membership further out. More specifically, in chip 2 we find about 4 times more variable stars outside $185''$ than predicted by the cluster's density profile. More details are provided in §5. The remaining chips will be the subject of a future paper, where the possible existence of extra-tidal stars in this cluster will also be examined. Finding charts for the M62 variable stars are presented in Figure 1.

We identified 66 of the 83 known variable stars discovered in previous studies (see the online catalogue by Clement et al. 2001, for a listing). Of the remaining 17 stars, we were un-

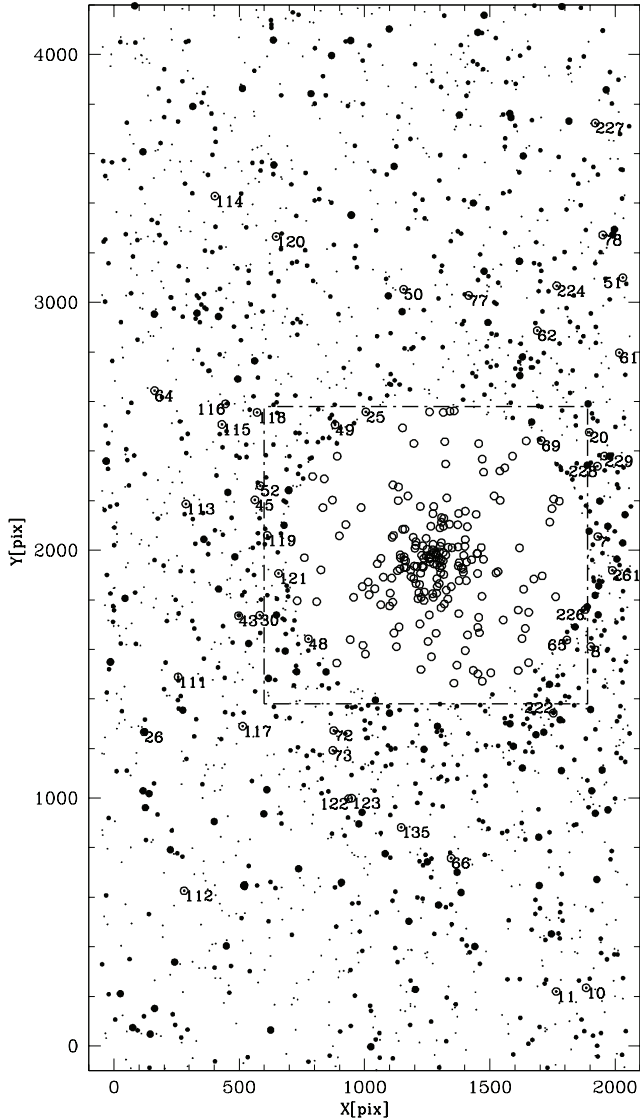


Figure 1. Finding chart for the variable stars in M62, based on the Warsaw 1.3m chip containing the cluster center. A zoom in around the dot-dashed region is shown in the next panel.

able to confirm variability for 2 of them, whereas the other 15 stars fall outside the fields that we have analyzed. On the other hand, Malakhova et al. (1997) find an additional 43 stars that they claim to lie in the instability strip of the cluster, and which are accordingly RR Lyrae candidates. In our study we were able to confirm the variability of 27 among their 43 candidates, with the remaining 16 stars being non-variable in our data.

Taking into account the 209 RR Lyrae stars detected in our study and the 15 additional RR Lyrae stars listed in Clement et al. (2001) which fall outside our studied fields, this gives a total of 224 RR Lyrae stars that are known so far in this cluster. For comparison, the most RR Lyrae-rich (in the sense of total number of RR Lyrae stars present) globular cluster known in our galaxy, M3 (NGC 5272), possesses a total of 230 reported RR Lyrae stars (Clementini et al. 2004), being followed by ω Centauri (NGC 5139), with a total of 178 RR Lyrae (Clement et al. 2001). Clearly, our detections place M62 among the most RR Lyrae-rich globular clusters known, and further analysis of the outer fields not included

in our study is not unlikely to give it the title of the most RR Lyrae-rich of all known globular star clusters (see also Contreras et al. 2005). In terms of the specific frequency of RR Lyrae variables, given by $S_{RR} = N_{RR} \times 10^{0.4(7.5+M_V)}$, and using for the cluster a $M_V = -9.19$ (as given in the Harris 1996 catalog, Feb. 2003 update), one finds $S_{RR} = 47.2$, which is very similar to the value $S_{RR} \approx 46$ originally reported by Contreras et al. (2005), and which again confirms the fact that M62 is an extremely RR Lyrae-rich object, since there are at present only 9 clusters with higher known S_{RR} , again according to the Harris catalog. In this sense, also noteworthy is the large number of LPV stars detected in the M62 field, with a total of 25 variables, 18 of which appear to be likely cluster members (see §5). According to the Clement et al. catalogue, previously the most LPV-rich of all globular clusters was ω Cen, with a total of 15 LPV stars. This suggests that M62 may also be the most LPV-rich known of all globular clusters (again in the sense of total number of LPV stars present).

While ISIS is very efficient in detecting variable stars in crowded fields, it presents the drawback of providing light curves in flux values relative to the composite frame. For this reason, ISIS does not provide light curves in standard magnitudes, and the composite image has to be processed independently for this purpose. To put our light curves in standard magnitude units, we followed the procedure recommended by Mochejska et al. (2001), for those variable stars which could be reliably measured in the reference frame. More specifically, the variable stars detected by ISIS were counter-identified with the B , V master catalogue of the reference frame, as obtained with DAOPHOT/ALLFRAME (Stetson 1987, 1994). Then, following the same procedure as in Mochejska et al., this allowed us to transform the light curves from differential fluxes into magnitude units.

While DAOPHOT/ALLFRAME represents an excellent tool to perform absolute photometry in the crowded regions found in globular clusters, it is still often the case that the variable stars located in the very crowded cluster center, as well as those located near bright and/or saturated objects (or close to the edges of the frames) will lack reliable photometry, even in our best seeing (reference) images. Therefore, among our sample of variable stars, 110 objects have differential flux light curves only, either because we could not measure their magnitudes on the reference frames, or because we consider that they lack reliable DAOPHOT/ALLFRAME photometry due to one or more of the aforementioned reasons.

Photometric properties and basic elements for the 245 variable stars in our study are presented in Table 1. Column 1 indicates the star's ID. Columns 2 and 3 provide the right ascension and declination (J2000 epoch), respectively, whereas column 4 gives our derived periods. Columns 5 and 6 list the derived amplitudes in the B and V bands, respectively. Columns 7 and 8, give the intensity-weighted mean B and V values, while column 9 shows the magnitude-weighted mean color. In column 10 we provide our derived reddening values for individual RRab stars (see §5 for more details), and finally column 11 indicates the star's variability type. We assigned a prefix "NV" to the newly identified objects, including the variable star candidates (NV84-NV110) from Malakhova et al. (1997). For the previously known 66 confirmed variables in our field, we obtain revised periods based on our data alone, since these new periods produce less scattered light curves than the old ones. The exception are

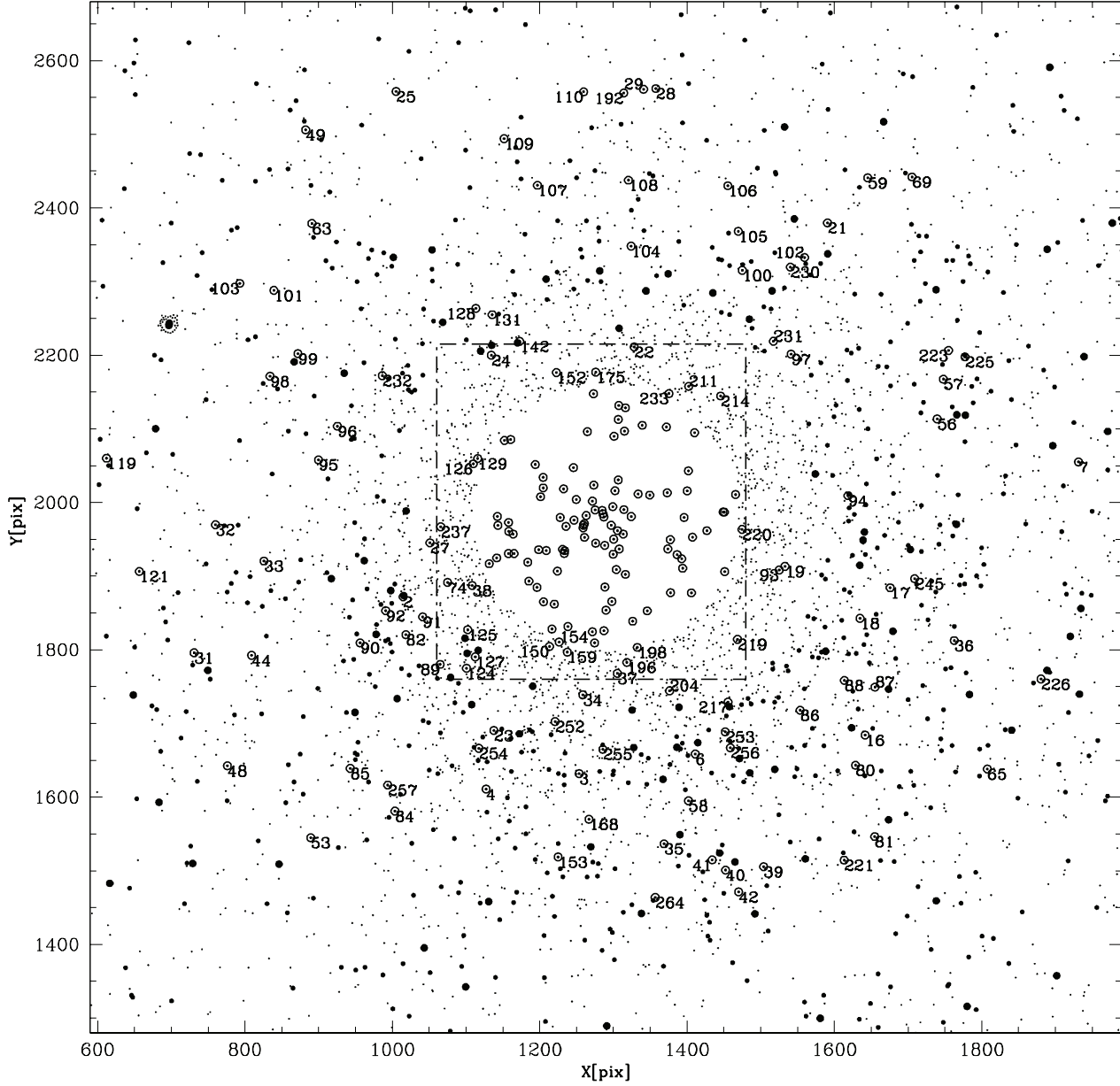


Figure 1, cont. Finding chart for the variable stars in M62. A zoom in around the dot-dashed region is shown in the next panel.

variables V4, V10, V11, V20, V23, V27, V38, V43, V45, V50, V52, V62, V62, V64, V66 and V78, where we adopt periods from the Clement et al. (2001) online catalog, since they provide good matches to our data. Sample light curves for the newly detected variables stars are shown in the Appendix, whereas the complete set of light curves can be found in the electronic version. The light curve data are provided, in machine-readable form, in Table 2.

3.1. Notes on Individual Variable Stars

V1, V3: Periods for these stars are not provided in the online Clement et al. (2001) catalog. The derived periods are based on an analysis of the CTIO images, even though only the LCO photometry is shown in the electronic version of the Appendix.

V77, NV117, NV149, NV155, NV166, NV174, NV176, NV178, NV186, NV197, NV202, NV204, NV207, NV225, NV229: These are short-period RRc stars with seemingly

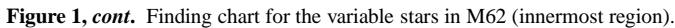
variable light curves. We have not been able to identify any source of spurious error in our photometry that could affect these stars in particular.

NV92, NV103, NV124, NV126, NV129, NV167, NV182, NV200, NV203, NV211, NV220: The derived periods are based on an analysis of the CTIO images, even though only the LCO light curves, which present significantly less scatter but do not constrain these stars' periods as tightly, are shown in the Appendix.

NV112, NV120, NV137, NV187, NV194: These stars present several aliases, and could not be detected in the CTIO data. The periods adopted are the ones that appear most consistent with an RRab type.

NV134, NV149: These stars present several aliases, and could not be detected in the CTIO data. The periods adopted are the ones that appear most consistent with an RRc type.

NV159, NV169: These stars show a curious mismatch in the light curves around phase 0.8 for the adopted periods. How-



NV170: This star presents several aliases, and an uncertain classification.

NV215: This star’s light curve presents an unusual behavior close to minimum light. A similar behavior is found in both the LCO and CTIO datasets, though the latter is considerably more noisy and contains fewer datapoints.

In the Fourier decomposition method, the light curves of ab-type pulsating stars are frequently fitted with a Fourier series of the form

where $w \equiv 2\pi/P$. The light curve shape is then quantified in terms of the lower-order ($j = 2-4$) coefficients $A_{j1} = A_j/A_1$

and $\phi_{j1} = \phi_j - j\phi_1$. In the case of c-type RR Lyrae, a similar procedure is followed, but a cosine decomposition is frequently used instead. In our study, we performed such Fourier decomposition of the RR Lyrae light curves, using $n = 10$, and adopting a sine series for the RRAb and a cosine series for the RRC stars. Amplitude ratios A_{j1} and phase differences ϕ_{j1} for the lower-order terms are provided in Tables 3 and 4 for the RRC and RRAb stars, respectively. For the RRAb stars we also give the Jurcsik-Kovács D_m value (Jurcsik & Kovács 1996, computed on the basis of their eq. 6 and Table 6), which is intended to differentiate RRAb stars with “regular” light curves from those with “anomalous” light curves, such as those presenting the Blazhko effect (but see Cacciari, Corwin, & Carney 2005, for a critical discussion of D_m as an indicator of the occurrence of the Blazhko phenomenon). In these tables, a colon symbol (“:”) indicates an uncertain value, whereas a double colon (“::”) indicates a very uncertain value, the latter being provided for complete-

ness only. The error in the ϕ_{31} coefficient was obtained from equation (16d) of Petersen (1986).

4.1. RRc Variables

Simon & Clement (1993) demonstrated, based on hydrodynamical models, that Fourier decomposition of RRc light curves can potentially provide a very useful technique for determining physical parameters of these stars. As a matter of fact, they have provided equations relating the masses, luminosities, temperatures, and even a “helium abundance parameter” of c-type RR Lyrae stars to their periods and ϕ_{31} values. Although these equations have been widely used in literature they must be used with some caution, since a combination of their equations for the RR Lyrae masses and luminosities gives results that are inconsistent with the period-mean density equation of stellar pulsation theory (Catelan 2004b; Deb & Singh 2010). Accordingly, while we still provide luminosities, masses and temperatures derived on the basis of the Simon & Clement relations, we warn the reader that these quantities cannot all be simultaneously valid, and should accordingly be used for comparison with similar work for other GCs only.

Based on the Simon & Clement (1993) relations, we find that an error of 0.2 in ϕ_{31} leads to an error of $\sim 0.03 M_{\odot}$ in mass and ~ 0.03 mag in (bolometric) magnitude, and so we apply this method only to RRc stars with errors in ϕ_{31} of 0.2 or less. We thus computed values of M/M_{\odot} , $\log(L/L_{\odot})$, $\log T_{\text{eff}}$, and “helium abundance parameter” y (which, as is well known, is not necessarily equal to the helium abundance Y ; see, e.g., Corwin et al. 2003); the resulting values are provided in Table 5, where we also provide $[\text{Fe}/\text{H}]_{\text{ZW84}}$ values (in the Zinn & West 1984, scale), based on the calibration recently provided by Morgan, Wahl, & Wieckhorst (2007), and M_V values, based on the calibration by Kovács (1998).

As the reader will readily notice, many of the mass values given in Table 5 are too low, approaching the mass of the degenerate helium core at the He flash ($\simeq 0.5 M_{\odot}$; see Catelan 2009, for a recent review). Such low mass values, which are not uncommon in the literature (e.g., Corwin et al. 2003, and reference therein) likely confirm the existence of a problem with the Simon & Clement (1993) calibration equations.

For the 21 retained RRc stars the unweighted mean values and standard deviations of the mass, log luminosity, effective temperature and helium parameter are $(0.533 \pm 0.04) M/M_{\odot}$, 1.663 ± 0.01 , (7413 ± 34) K, and 0.293 ± 0.003 , respectively. The mean metallicity, in turn, is found to be $[\text{Fe}/\text{H}]_{\text{ZW84}} = -1.23 \pm 0.09$.

According to the Kovács (1998) calibration, the mean absolute magnitude in V of these RRc stars turns out to be $\langle M_V \rangle = 0.714 \pm 0.033$. Since for these stars we also have a $\langle V \rangle = 16.44 \pm 0.06$ mag (standard error of the mean), this gives for the cluster an apparent distance modulus of $(m - M)_V = 15.73 \pm 0.068$ mag.

4.2. RRab Variables

In a series of papers, the Hungarian team has provided a calibration of several physical parameters of “well-behaved” (as indicated by the aforementioned D_m parameter) ab-type RR Lyrae stars as a function of their Fourier decomposition parameters (e.g., Jurcsik & Kovács 1996; Jurcsik 1998; Kovács & Walker 1999, 2001). Unlike the approach adopted by Simon & Clement (1993) for the RRc stars, their method does not rely on hydrodynamical models for the calibration. Following the same approach as described in detail in

Table 4
Fourier Coefficients for RRAb Variables in M62

| ID | A_{21} | A_{31} | A_{41} | ϕ_{21} | ϕ_{31} | ϕ_{41} | D_m |
|---------|----------|----------|----------|-------------|-------------|-------------|--------|
| V4 | 0.452 | 0.315 | 0.256 | 2.392 | 4.780 | 1.046 | 4.9 |
| V6: | 0.455 | 0.301 | 0.220 | 2.351 | 4.929 | 1.237 | 2.7 |
| V7 | 0.523 | 0.341 | 0.200 | 2.638 | 5.468 | 2.141 | 2.2 |
| V8 | 0.520 | 0.356 | 0.218 | 2.354 | 5.130 | 1.563 | 3.5 |
| V10 | 0.511 | 0.351 | 0.234 | 2.363 | 5.101 | 1.526 | 1.2 |
| V11:: | 0.452 | 0.228 | 0.138 | 2.738 | 5.493 | 1.910 | 6.1 |
| V16 | 0.500 | 0.336 | 0.171 | 2.624 | 5.368 | 2.132 | 5.9 |
| V17 | 0.555 | 0.380 | 0.251 | 2.369 | 5.059 | 1.556 | 3. |
| V18 | 0.492 | 0.340 | 0.221 | 2.378 | 5.153 | 1.645 | 3.1 |
| V20 | 0.476 | 0.394 | 0.257 | 2.281 | 4.878 | 1.087 | 3.4 |
| V21 | 0.476 | 0.364 | 0.221 | 2.218 | 4.772 | 1.032 | 2.4 |
| V23 | 0.547 | 0.392 | 0.238 | 2.084 | 4.474 | 0.628 | 42.9 |
| V24 | 0.508 | 0.344 | 0.264 | 2.377 | 5.204 | 1.608 | 6.2 |
| V25 | 0.473 | 0.343 | 0.216 | 2.225 | 4.796 | 1.142 | 1.7 |
| V26 | 0.569 | 0.288 | 0.186 | 2.519 | 5.227 | 1.701 | 2.9 |
| V27 | 0.478 | 0.353 | 0.224 | 2.288 | 4.891 | 1.261 | 2.5 |
| V28:: | 0.786 | 0.321 | 1.381 | 0.782 | 5.934 | 5.959 | 1617.8 |
| V29 | 0.535 | 0.317 | 0.251 | 2.422 | 5.142 | 1.620 | 4.6 |
| V31: | 0.523 | 0.381 | 0.236 | 2.268 | 4.947 | 1.152 | 4. |
| V32 | 0.517 | 0.330 | 0.221 | 2.466 | 5.297 | 1.863 | 1.7 |
| V33 | 0.549 | 0.341 | 0.209 | 2.523 | 5.313 | 2.004 | 2.5 |
| V34 | 0.529 | 0.314 | 0.188 | 2.559 | 5.264 | 1.868 | 1.3 |
| V35 | 0.487 | 0.339 | 0.223 | 2.363 | 5.076 | 1.557 | 0.6 |
| V36 | 0.459 | 0.278 | 0.105 | 2.646 | 5.617 | 2.238 | 2.9 |
| V39 | 0.429 | 0.211 | 0.080 | 2.610 | 5.735 | 2.845 | 7.2 |
| V41 | 0.495 | 0.306 | 0.177 | 2.529 | 5.391 | 2.071 | 1.6 |
| V43 | 0.529 | 0.342 | 0.212 | 2.433 | 5.177 | 1.736 | 2.2 |
| V44 | 0.392 | 0.211 | 0.092 | 2.370 | 4.808 | 0.977 | 46.9 |
| V48 | 0.444 | 0.271 | 0.088 | 2.812 | 5.914 | 2.697 | 127.6 |
| V49 | 0.517 | 0.313 | 0.197 | 2.338 | 5.090 | 1.596 | 1. |
| V50:: | 1.070 | 1.287 | 1.461 | 1.771 | 3.458 | 5.002 | 590. |
| V52:: | 1.178 | 1.808 | 2.167 | 1.873 | 3.279 | 4.364 | 3585.7 |
| V56 | 0.501 | 0.314 | 0.194 | 2.472 | 5.314 | 1.902 | 1.5 |
| V57 | 0.478 | 0.304 | 0.170 | 2.441 | 5.197 | 1.637 | 2.1 |
| V58:: | 1.058 | 0.888 | 0.674 | 4.873 | 3.491 | 2.047 | 204.9 |
| V59 | 0.531 | 0.334 | 0.191 | 2.567 | 5.404 | 2.086 | 2.8 |
| V62 | 0.516 | 0.330 | 0.212 | 2.423 | 5.184 | 1.693 | 1.5 |
| V63 | 0.461 | 0.264 | 0.102 | 2.741 | 5.692 | 2.740 | 5.6 |
| V64: | 0.450 | 0.287 | 0.163 | 2.266 | 4.611 | 1.000 | 7.1 |
| V72 | 0.418 | 0.231 | 0.121 | 2.349 | 5.051 | 1.265 | 39.6 |
| V78: | 0.491 | 0.318 | 0.168 | 2.682 | 5.546 | 2.297 | 3.9 |
| V80: | 0.445 | 0.229 | 0.138 | 2.541 | 5.285 | 2.428 | 18. |
| V81 | 0.528 | 0.360 | 0.216 | 2.411 | 5.153 | 1.634 | 1.7 |
| V82 | 0.489 | 0.292 | 0.145 | 2.536 | 5.400 | 2.278 | 2.7 |
| NV84 | 0.388 | 0.170 | 0.043 | 2.774 | 5.980 | 2.844 | 109. |
| NV87 | 0.288 | 0.115 | 0.059 | 2.774 | 5.846 | 3.653 | 118.9 |
| NV88 | 0.496 | 0.301 | 0.137 | 2.608 | 5.508 | 2.222 | 1.7 |
| NV93 | 0.519 | 0.368 | 0.230 | 2.429 | 5.132 | 1.648 | 2. |
| NV95: | 0.466 | 0.342 | 0.203 | 2.138 | 4.648 | 0.846 | 45.6 |
| NV96 | 0.481 | 0.359 | 0.224 | 2.259 | 4.924 | 1.232 | 2.8 |
| NV97 | 0.509 | 0.313 | 0.203 | 2.445 | 5.274 | 1.820 | 2.1 |
| NV98 | 0.501 | 0.328 | 0.207 | 2.486 | 5.323 | 1.812 | 1.8 |
| NV99:: | 0.426 | 0.259 | 0.149 | 2.753 | 6.272 | 3.011 | 11.7 |
| NV102 | 0.421 | 0.229 | 0.103 | 2.646 | 5.465 | 2.292 | 1.3 |
| NV103:: | 0.872 | 0.726 | 0.556 | 4.808 | 3.251 | 1.729 | 298.9 |
| NV105 | 0.540 | 0.363 | 0.259 | 2.371 | 5.087 | 1.546 | 4.9 |
| NV106 | 0.424 | 0.302 | 0.220 | 2.336 | 4.881 | 1.328 | 4.2 |
| NV107 | 0.479 | 0.307 | 0.140 | 2.555 | 5.462 | 2.088 | 3.6 |
| NV109: | 0.461 | 0.293 | 0.144 | 2.626 | 5.606 | 2.385 | 8.8 |
| NV112:: | 0.936 | 0.839 | 0.730 | 1.672 | 3.466 | 5.340 | 2030.9 |
| NV113:: | 0.359 | 0.448 | 0.176 | 2.170 | 4.619 | 1.514 | 16.7 |
| NV116 | 0.375 | 0.165 | 0.066 | 2.643 | 5.776 | 2.954 | 7.8 |
| NV120:: | 0.872 | 0.741 | 0.649 | 1.613 | 3.284 | 4.894 | 1632.9 |
| NV124:: | 0.815 | 0.698 | 0.548 | 4.734 | 3.247 | 1.697 | 276.1 |
| NV127 | 0.529 | 0.321 | 0.248 | 2.307 | 5.049 | 1.395 | 3.5 |
| NV135 | 0.460 | 0.300 | 0.107 | 2.636 | 5.420 | 2.623 | 108.4 |
| NV136 | 0.544 | 0.330 | 0.173 | 2.695 | 5.440 | 2.250 | 7.7 |
| NV150 | 0.343 | 0.146 | 0.019 | 2.535 | 5.053 | 1.546 | 43.9 |
| NV160 | 0.525 | 0.358 | 0.225 | 2.394 | 5.272 | 1.772 | 3.2 |
| NV168 | 0.261 | 0.088 | 0.023 | 2.864 | 5.627 | 5.322 | 115.6 |
| NV194:: | 0.924 | 0.775 | 0.623 | 1.644 | 3.280 | 4.853 | 762.4 |
| NV198: | 0.561 | 0.319 | 0.168 | 2.317 | 5.101 | 1.824 | 8.9 |
| NV210 | 0.466 | 0.335 | 0.183 | 2.339 | 4.859 | 1.265 | 7.5 |
| NV214 | 0.502 | 0.328 | 0.167 | 2.489 | 5.325 | 1.987 | 1.8 |
| NV218: | 0.443 | 0.271 | 0.144 | 2.253 | 4.759 | 0.771 | 41.9 |
| NV219 | 0.461 | 0.249 | 0.112 | 2.816 | 5.976 | 2.706 | 7.8 |
| NV223 | 0.519 | 0.337 | 0.208 | 2.386 | 5.101 | 1.584 | 1.1 |
| NV226 | 0.511 | 0.303 | 0.161 | 2.663 | 5.588 | 2.349 | 2.2 |
| NV227 | 0.486 | 0.326 | 0.195 | 2.304 | 4.796 | 1.174 | 44.8 |
| NV228: | 0.329 | 0.113 | 0.031 | 2.680 | 5.805 | 3.165 | 132.3 |

Table 5
Physical Parameters derived for RRc Variables in M62

| ID | M/M_{\odot} | $\log(L/L_{\odot})$ | $\log T_{\text{eff}}$ | y | [Fe/H] | $\langle M_V \rangle$ |
|-------|---------------|---------------------|-----------------------|-------------|--------------|-----------------------|
| V30 | 0.573 | 1.681 | 3.868 | 0.282 | -1.418 | 0.733 |
| V40 | 0.525 | 1.658 | 3.871 | 0.292 | -1.180 | 0.686 |
| V53 | 0.588 | 1.651 | 3.873 | 0.290 | -1.207 | 0.699 |
| V69 | 0.496 | 1.658 | 3.870 | 0.294 | -1.136 | 0.725 |
| NV85 | 0.492 | 1.663 | 3.869 | 0.293 | -1.173 | 0.719 |
| NV86 | 0.524 | 1.646 | 3.872 | 0.295 | -1.082 | 0.746 |
| NV91 | 0.494 | 1.660 | 3.869 | 0.293 | -1.154 | 0.714 |
| NV100 | 0.608 | 1.651 | 3.874 | 0.289 | -1.226 | 0.736 |
| NV101 | 0.534 | 1.666 | 3.870 | 0.289 | -1.259 | 0.689 |
| NV108 | 0.526 | 1.655 | 3.871 | 0.293 | -1.161 | 0.760 |
| NV110 | 0.490 | 1.678 | 3.867 | 0.288 | -1.297 | 0.652 |
| NV115 | 0.609 | 1.654 | 3.873 | 0.288 | -1.253 | 0.736 |
| NV118 | 0.539 | 1.661 | 3.870 | 0.290 | -1.224 | 0.723 |
| NV119 | 0.519 | 1.674 | 3.868 | 0.288 | -1.305 | 0.719 |
| NV121 | 0.573 | 1.654 | 3.872 | 0.290 | -1.209 | 0.756 |
| NV123 | 0.500 | 1.650 | 3.871 | 0.296 | -1.075 | 0.730 |
| NV131 | 0.517 | 1.667 | 3.869 | 0.290 | -1.247 | 0.703 |
| NV140 | 0.435 | 1.694 | 3.862 | 0.287 | -1.347 | 0.613 |
| NV153 | 0.527 | 1.671 | 3.869 | 0.288 | -1.293 | 0.708 |
| NV175 | 0.586 | 1.660 | 3.872 | 0.288 | -1.274 | 0.734 |
| NV224 | 0.538 | 1.683 | 3.867 | 0.284 | -1.397 | 0.713 |
| mean | 0.533±0.043 | 1.663±0.012 | 3.870±0.002 | 0.290±0.003 | -1.234±0.009 | 0.714±0.033 |

Table 6
Physical Parameters Derived for RRAb Variables in M62

| ID | [Fe/H] ₉₅ | $\langle M_V \rangle$ | $\langle B-V \rangle$ | $\log T_{\text{eff}}^{(B-V)}$ | $\langle V-I \rangle$ | $\log T_{\text{eff}}^{(V-I)}$ | $\langle V-K \rangle$ | $\log T_{\text{eff}}^{(V-K)}$ |
|-------------------|----------------------|-----------------------|-----------------------|-------------------------------|-----------------------|-------------------------------|-----------------------|-------------------------------|
| V4 | -1.527 | 0.782 | 0.328 | 3.814 | 0.479 | 3.814 | 1.110 | 3.810 |
| V7 | -0.725 | 0.840 | 0.343 | 3.815 | 0.498 | 3.808 | 1.057 | 3.813 |
| V8 | -1.011 | 0.843 | 0.337 | 3.815 | 0.491 | 3.810 | 1.058 | 3.814 |
| V10 | -1.049 | 0.808 | 0.322 | 3.819 | 0.472 | 3.815 | 1.044 | 3.816 |
| V17 | -1.089 | 0.830 | 0.334 | 3.815 | 0.487 | 3.811 | 1.064 | 3.814 |
| V18 | -0.934 | 0.848 | 0.330 | 3.818 | 0.481 | 3.813 | 1.041 | 3.816 |
| V20 | -1.023 | 0.867 | 0.316 | 3.822 | 0.464 | 3.817 | 0.991 | 3.822 |
| V21 | -1.047 | 0.868 | 0.301 | 3.828 | 0.444 | 3.823 | 0.974 | 3.824 |
| V25 | -0.993 | 0.875 | 0.296 | 3.830 | 0.439 | 3.824 | 0.969 | 3.824 |
| V26 | -0.012 | 1.047 | 0.286 | 3.842 | 0.424 | 3.827 | 0.824 | 3.837 |
| V27 | -0.882 | 0.868 | 0.293 | 3.831 | 0.435 | 3.825 | 0.952 | 3.826 |
| V29 | -1.170 | 0.768 | 0.324 | 3.817 | 0.475 | 3.814 | 1.082 | 3.812 |
| V32 | -0.869 | 0.843 | 0.338 | 3.815 | 0.493 | 3.809 | 1.059 | 3.814 |
| V33 | -0.980 | 0.813 | 0.345 | 3.812 | 0.501 | 3.807 | 1.097 | 3.810 |
| V34 | -1.104 | 0.772 | 0.334 | 3.814 | 0.487 | 3.811 | 1.101 | 3.810 |
| V35 | -1.065 | 0.847 | 0.337 | 3.815 | 0.490 | 3.810 | 1.069 | 3.813 |
| V36 | -1.004 | 0.774 | 0.369 | 3.803 | 0.532 | 3.799 | 1.164 | 3.802 |
| V41 | -0.802 | 0.862 | 0.349 | 3.812 | 0.506 | 3.806 | 1.078 | 3.811 |
| V43 | -1.114 | 0.828 | 0.350 | 3.809 | 0.508 | 3.806 | 1.110 | 3.809 |
| V49 | -1.122 | 0.825 | 0.335 | 3.815 | 0.488 | 3.811 | 1.083 | 3.812 |
| V56 | -0.919 | 0.837 | 0.344 | 3.813 | 0.500 | 3.808 | 1.081 | 3.811 |
| V57 | -1.048 | 0.831 | 0.342 | 3.813 | 0.497 | 3.809 | 1.084 | 3.811 |
| V59 | -0.892 | 0.828 | 0.351 | 3.810 | 0.509 | 3.805 | 1.096 | 3.809 |
| V62 | -1.021 | 0.834 | 0.340 | 3.814 | 0.494 | 3.809 | 1.076 | 3.812 |
| V81 | -0.970 | 0.843 | 0.335 | 3.816 | 0.488 | 3.811 | 1.052 | 3.815 |
| V82 | -0.821 | 0.875 | 0.359 | 3.809 | 0.518 | 3.803 | 1.107 | 3.808 |
| NV88 | -0.762 | 0.854 | 0.357 | 3.809 | 0.516 | 3.803 | 1.093 | 3.809 |
| NV93 | -1.113 | 0.824 | 0.344 | 3.812 | 0.500 | 3.808 | 1.091 | 3.811 |
| NV96 | -0.930 | 0.874 | 0.309 | 3.826 | 0.454 | 3.820 | 0.979 | 3.823 |
| NV97 | -0.915 | 0.849 | 0.343 | 3.813 | 0.498 | 3.808 | 1.072 | 3.812 |
| NV98 | -0.909 | 0.836 | 0.345 | 3.813 | 0.501 | 3.807 | 1.073 | 3.812 |
| NV102 | -1.089 | 0.799 | 0.368 | 3.803 | 0.531 | 3.800 | 1.181 | 3.801 |
| NV105 | -1.002 | 0.837 | 0.327 | 3.818 | 0.478 | 3.813 | 1.040 | 3.816 |
| NV106 | -1.189 | 0.811 | 0.305 | 3.824 | 0.451 | 3.821 | 1.038 | 3.817 |
| NV107 | -0.781 | 0.868 | 0.360 | 3.809 | 0.519 | 3.803 | 1.090 | 3.810 |
| NV127 | -1.120 | 0.783 | 0.310 | 3.823 | 0.457 | 3.819 | 1.037 | 3.817 |
| NV160 | -0.879 | 0.810 | 0.325 | 3.820 | 0.476 | 3.814 | 1.033 | 3.816 |
| NV214 | -1.043 | 0.817 | 0.356 | 3.808 | 0.514 | 3.804 | 1.124 | 3.807 |
| NV223 | -1.048 | 0.836 | 0.333 | 3.816 | 0.485 | 3.812 | 1.063 | 3.814 |
| NV226 | -0.921 | 0.782 | 0.359 | 3.807 | 0.519 | 3.802 | 1.138 | 3.805 |
| mean ^a | -0.997±0.144 | 0.830±0.030 | 0.336±0.019 | 3.815±0.006 | 0.489±0.024 | 3.811±0.006 | 1.068±0.049 | 3.813±0.005 |

^a Excluding V26.

Corwin et al. (2003), we obtain the metallicities, mean colors, and associated temperatures that are listed in Table 6, for 40 RRab stars with $D_m \leq 5$ (see also Clement & Shelton 1997). Note that V26 is most likely a field star (see §5), and therefore was not taken into account when computing the average values for the cluster, as indicated in this table.

Note that the $[\text{Fe}/\text{H}]$ values derived in this way are actually in the scale of Jurcsik (1995). The latter is related to the more traditional Zinn & West (1984) scale by $[\text{Fe}/\text{H}]_{\text{J95}} = 1.431 [\text{Fe}/\text{H}]_{\text{ZW84}} + 0.880$. Therefore, the mean metallicity $[\text{Fe}/\text{H}]_{\text{J95}} = -0.997$ that was derived for the cluster in Table 6 translates into a metallicity value $[\text{Fe}/\text{H}]_{\text{ZW84}} = -1.31$ in the Zinn & West scale. This agrees very well with the value adopted for the cluster by Harris (1996), namely $[\text{Fe}/\text{H}]_{\text{ZW84}} = -1.29$, in his catalog of globular cluster parameters (2003 update), as well as with the value derived from the RRc by using the Morgan et al. (2007) calibration, namely $[\text{Fe}/\text{H}]_{\text{ZW84}} = -1.23$ (§4.1).

Likewise, we obtain a mean absolute magnitude of $\langle M_V \rangle = 0.83 \pm 0.03$ mag for the RRab stars in the cluster. The faint HB is a reflection of the adoption of the Baade-Wesselink luminosity zero point in the calibration of this method (see Jurcsik & Kovács 1999, for a discussion). For the same set of 39 RRab used to derive this value, we also find $\langle V_{RR} \rangle = 16.260 \pm 0.03$ mag (standard error of the mean), which is also in very good agreement with the value of 16.25 mag adopted in the 2003 edition of the Harris (1996) catalog. This implies an apparent distance modulus of $(m-M)_V = 15.43 \pm 0.04$ mag for M62, which is significantly shorter (by 0.21 mag) than the value provided in the Harris catalog, and by an even wider margin (i.e., 0.3 mag) than the value obtained in §4.1 on the basis of the Kovács (1998) M_V calibration for the c-type RR Lyrae. We ascribe these differences to the faint zero point adopted in the original M_V calibrations. If we adopt instead the more recent calibration of the RR Lyrae absolute magnitude-metallicity relation provided by Catelan & Cortés (2008), and the metallicity value for M62 derived above ($[\text{Fe}/\text{H}]_{\text{ZW84}} = -1.31$), we find $M_V(\text{RR}) = 0.68 \pm 0.14$, and an apparent distance modulus of $(m-M)_V = 15.58 \pm 0.14$, which is much more consistent with the value reported in the Harris catalog (being shorter by only 0.06 mag). Using a reddening value of $E(B-V) = 0.47$ (from Harris 1996) and a standard extinction law with $A_V/E(B-V) = 3.1$, this implies a distance modulus $(m-M)_0 = 14.12 \pm 0.14$, which corresponds to a distance of 6.7 ± 1 kpc.

Note that a distance modulus for the cluster may also be obtained on the basis of our detected type II Cepheids, namely V2 and V73, using equation (3) in Pritzl et al. (2003). In this way, we obtain for distance moduli of $(m-M)_V = 15.04$ and $(m-M)_V = 15.57$ mag, respectively – giving an average distance modulus of $(m-M)_V \approx 15.31 \pm 0.26$ mag. Given the large error bar, this value is not inconsistent with the one derived on the basis of the RR Lyrae stars.

As noted by Contreras et al. (2005), M62 may harbor long-period RRc's (see their Fig. 2), which are exceedingly rare among Galactic globular clusters (see Catelan 2004b, for a review). In order to check the pulsation status of the two candidate long-period RRc stars that we have found in the cluster, namely NV104 and NV171, we have used several diagnostics from Simon & Teays (1982) and Clement & Shelton (1997), who have shown that the RRab and RRc stars occupy distinctly different positions in the A_{21} , ϕ_{21} plane in particular, as well as the Sk (skewness) parameter defined by

Stellingwerf & Donohoe (1987). Figure 2 shows that, for the RR Lyrae with clean light curves in our sample, most of the ab-type RR Lyrae do indeed have values of $A_{21} > 0.3$, and vice-versa for the RRc stars. Similarly, most of the RRc stars have $Sk < 2$, whereas most of the ab-type RR Lyrae have $Sk > 2$. As can be seen, in all plots but the one showing ϕ_{31} as a function of $\log P$ one finds that the positions of these two stars are closer to the locus occupied by RRc than RRab stars. The atypical position of NV104 and NV171 in the $\phi_{31} - \log P$ plane is particularly intriguing, in view of the fact that, if these stars are indeed c-type RR Lyrae, their periods would clearly be longer than the vast majority of even the ab-type RR Lyrae in the cluster.

5. CMD AND REDDENING

On the basis of our ALLFRAME reductions, we were able to obtain a deep CMD for M62, which we show in Figure 3. The CMD properties will be discussed in detail in a forthcoming paper (Contreras et al. 2010, in preparation), and we show it here with the main purpose of verifying whether the positions of the variable stars that were detected in our field are consistent with cluster membership – which is clearly confirmed for the vast majority of the stars. One obvious exception is provided by the RRab star V26, which is clearly a foreground field RR Lyrae. That V26 is a field star is also suggested by the near-solar metallicity derived for it on the basis of its Fourier decomposition parameters (see Table 6). The membership status of NV224 and NV227, on the other hand, is less clear, for while their CMD positions suggest that they may be RR Lyrae stars in the cluster background, their Fourier-based metallicities do not clearly point to them as being anomalous. In like vein, their metallicity values, as derived using the Jurcsik (1995) and Morgan et al. (2007) techniques, suggest $[\text{Fe}/\text{H}]$ values of -1.40 (for NV224) and -1.35 (for NV227), neither of which is clearly inconsistent with the cluster's metallicity. The derived $[\text{Fe}/\text{H}]$ value for NV227 should be taken with due caution though, in view of the star's fairly large D_m value (see Table 4).

Unfortunately, as can be seen from Figure 3 (left panel), the cluster CMD is severely affected by differential reddening, which is not unexpected in view of M62's large foreground reddening and low Galactic latitude. On the other hand, the presence of a large number of RR Lyrae variable stars across the face of the cluster can provide us with a handle of this problem, since RR Lyrae stars can themselves provide dependable reddening estimates, particularly on the basis of the colors of the ab-type RR Lyrae at minimum light (e.g., Blanco 1992).

We have applied the Blanco (1992) technique to 71 stars in our RRab sample, and thus obtained a two-dimensional reddening map across the face of the cluster. In this case, we adopted the same $[\text{Fe}/\text{H}]$ value for all the RRab stars, namely $[\text{Fe}/\text{H}] = -1.31$, as derived from Fourier decomposition (§4.2), and which is very similar to the value listed in the Harris (1996) catalog, namely $[\text{Fe}/\text{H}] = -1.29$. We then experimented with several different techniques for interpolating on this map to obtain reddening values for individual cluster stars, finally opting for a LOESS smoother (Cleveland 1979; Cleveland & Devlin 1988). That this provided very good results can readily be appreciated by comparing the differential reddening-corrected CMD (Fig. 3, right panel) with the original one. A zoomed-in plot around the HB region is shown in Figure 4.

We also note the anomalous positions of stars NV225 (an

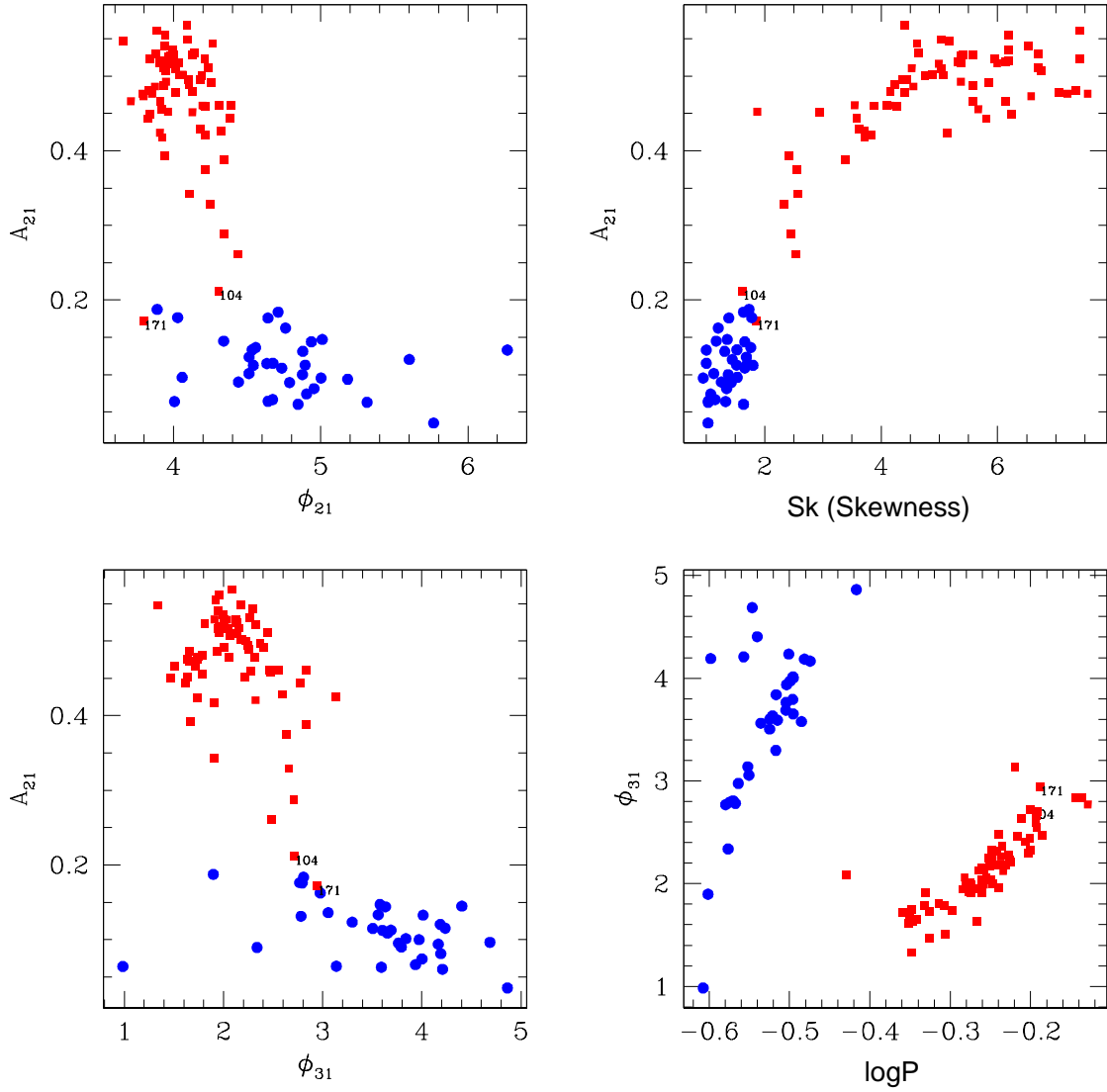


Figure 2. Pulsation mode diagnostics for RR Lyrae stars. In all panels, circles indicate c-type RR Lyrae stars, whereas squares indicate ab-type RR Lyrae. Some of the variables discussed in the text are indicated by their V (or NV) number.

RRc) and V23 (an RRab) in the CMD. Not only are these stars brighter and redder than other RR Lyrae stars in the cluster, but also – and importantly – they also present peculiarly large A_B/A_V amplitude ratios. This strongly suggests that they are blended with redder companions.

In order to verify whether those variable stars for which we were not able to obtain average magnitudes and colors over the full pulsation cycle belong to M62, we have included a third CMD in Figure 5. In this case, the variable stars were simply identified in the photometry catalog and plotted in the CMD using mean magnitudes and colors computed as simple averages of the available photometric data. While this necessarily leads to increased scatter in the derived CMD positions (as is particularly obvious around the RR Lyrae region of the CMD), it also allows us to investigate the likelihood that these stars may be cluster members. To further aid us in this direction, we overplot in Figure 5 two model isochrones from the

Pietrinferni et al. (2006) set, computed for a chemical composition consistent with that of the cluster (in green, reddened and vertically shifted in order to match the HB of the cluster) and for a chemical composition consistent with a bulge field at the position of the cluster (in red, plotted using the same distance modulus as obtained for the cluster). From their CMD positions, it appears that most of the LPV stars discovered in this paper (i.e., 18 out of 25) are likely cluster members, with only a few LPV candidates likely belonging to the bulge. Note also that NV231, which we originally classified as an LPV candidate, may actually be more properly classified as a background type II Cepheid, judging from its position in the CMD.

Finally, we note that all those RR Lyrae stars for which we derived metallicities using Fourier decomposition, and which are located inside the cluster’s tidal radius, present chemical abundances that are compatible with M62 membership, ex-

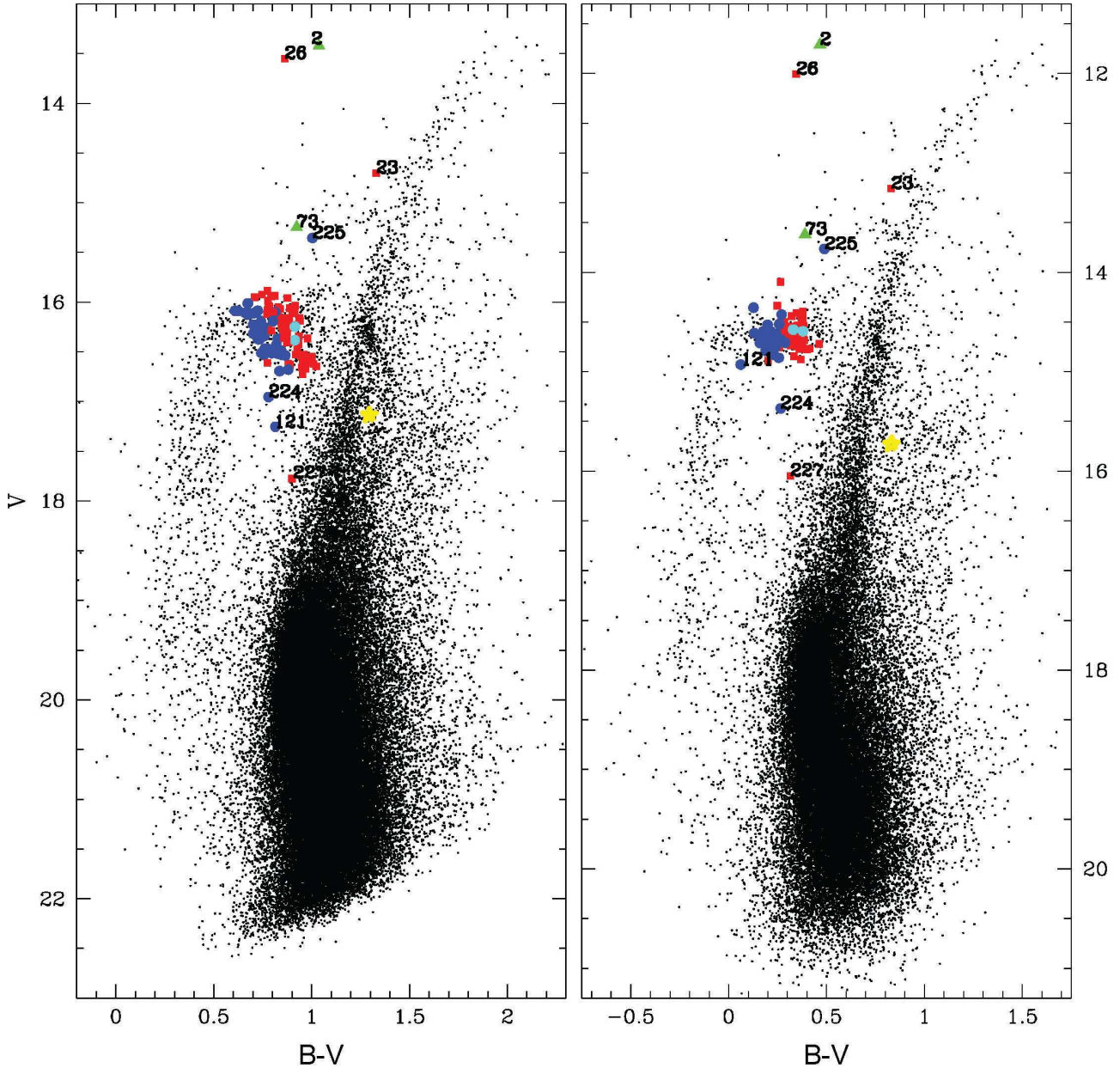


Figure 3. Our derived CMD for the cluster, with the mean values for the detected variable stars overplotted. Circles indicate c-type RR Lyrae, squares ab-type RR Lyrae, and triangles type II Cepheids. The diagram on the right is the same as the one on the left, but with differential reddening accounted for as described in the text.

cept for the already cited case of V26 – thus suggesting that most of the variable star candidates in the cluster outskirts are indeed cluster members.

6. ON THE OOSTERHOFF TYPE OF M62

The Oosterhoff phenomenon is of great astrophysical importance, given the information that it carries on the early formation history of the Milky Way and its neighboring galaxies (e.g., Kuehn et al. 2008; Catelan 2009; Moretti et al. 2009, and references therein), and (increasingly) in the Andromeda system (e.g., Contreras et al. 2008; Clementini et al. 2009; Fiorentino et al. 2010; Sarajedini et al. 2009, and references therein). As recently summarized by Catelan (2009), there is a general tendency for bona-fide Galactic globular clusters to present the so-called Oosterhoff dichotomy, i.e., a sharp division between Oosterhoff type I (OoI) systems, with $\langle P_{ab} \rangle \approx 0.55$ d, and Oosterhoff type II (OoII) systems, with

$\langle P_{ab} \rangle \approx 0.65$ d, with exceedingly few Galactic globulars occupying the range between $0.58 \lesssim \langle P_{ab}(d) \rangle \lesssim 0.62$. On the contrary, nearby extragalactic globular clusters and dwarf galaxies occupy *preferentially* the latter average period interval, thus clearly revealing a difference in (early) formation history between bona-fide Galactic and nearby extragalactic systems.

As discussed by Contreras et al. (2005), there is at present some debate as to whether the Oosterhoff type of a globular cluster is determined chiefly by the morphology of the HB (Clement & Shelton 1999), or whether metallicity plays an important role as well – as would be supported by theoretical calculations that indicate different evolutionary paths for HB stars of different metallicities but similar zero-age HB (ZAHB) temperatures, and thus a different efficiency of production of stars evolved away from the ZAHB as a function of metallicity (see §5.7 in Pritzl et al. 2002, and references

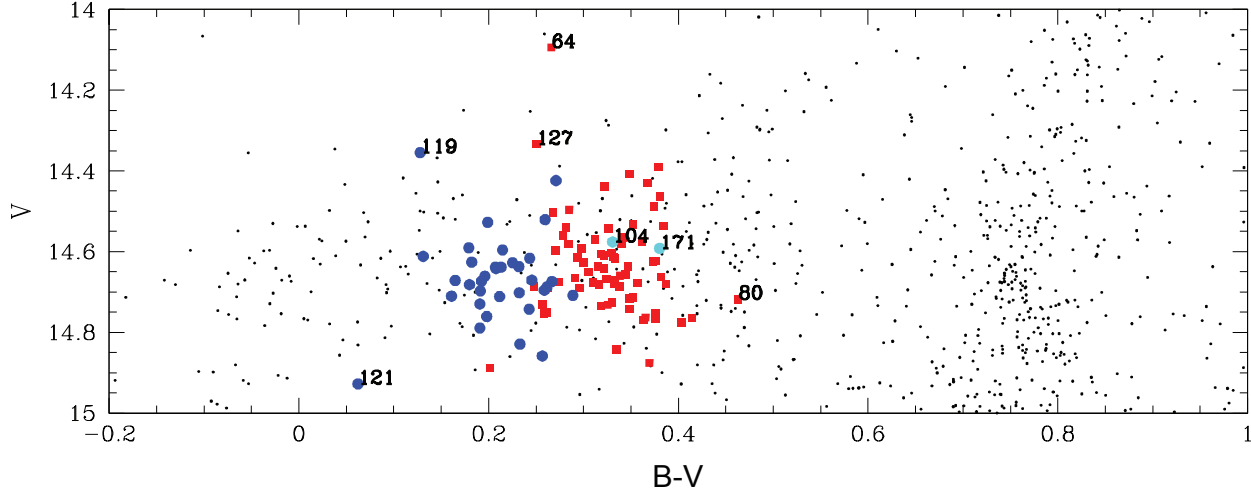


Figure 4. As in Figure 3 (right panel), but zooming in around the HB.

therein). As noted by Contreras et al., M62 provides a near-ideal test of the relative importance of HB morphology and metallicity in defining the Oosterhoff type of a globular cluster, given that the cluster possesses a predominantly blue HB, as in the case of most OoII clusters, but is also a fairly metal-rich object, as in the case of most OoI clusters.

Here we confirm the preliminary results by Contreras et al. (2005), finding that the mean periods of the ab-type RR Lyrae in M62 support an OoI classification for the cluster, thus clearly showing that, at least in the case of M62, metallicity is the dominant factor that defines the Oosterhoff type. Indeed, let us assume, as a first approximation, that all of our detected variables are cluster members. In this case, and taking our homogeneous sample of 133 RRab's and 76 RRC's into account, we derive for the cluster average pulsation periods of $\langle P_{ab} \rangle = 0.547$ d and $\langle P_c \rangle = 0.302$ d, thus confirming the preliminary values reported by Contreras et al., which are quite typical for OoI systems. If the 5 RRab and 3 RRC with uncertain classification – namely, NV112, NV120, NV137, NV187, NV194 and NV134, NV149 – are removed, we obtain $\langle P_{ab} \rangle = 0.548$ d and $\langle P_c \rangle = 0.301$ d. As we have seen, the membership status for the RRab stars V26 and NV227 and the RRC variable NV224 is also questionable; if we further remove these stars from the final tally, we obtain $\langle P_{ab} \rangle = 0.550$ d (126 RRab stars) and $\langle P_c \rangle = 0.302$ d (73 RRC stars).

As discussed by Catelan et al. (2010, in preparation), $\langle P_{ab} \rangle$ and $P_{ab,min}$ are the two quantities that most strongly define the Oosterhoff type. For M62, the shortest-period RRab is NV188, and thus $P_{ab,min} = 0.436$ d – which again clearly indicates an OoI classification.

As a matter of fact, as shown in Figure 6, the detailed period distribution is quite similar for both the prototypical OoI globular cluster M3 and M62, with the main differences being a somewhat shorter mean period for the RRC stars in M62 and a slightly broader distribution of ab-type periods. The period-amplitude diagram may also provide further insight into these differences, in addition to useful information regarding the Oosterhoff classification of stellar systems (e.g., Cacciari et al. 2005, and references therein). How does this diagram look in the case of M62, once those RRab stars identified as peculiar (i.e., with $D_m > 5.0$) have been removed?

The answer is provided in Figure 7, where both the $A_V - \log P$ (upper panel) and $A_B - \log P$ (lower panel) planes are

shown. In these figures, we also provide reference lines for OoI and OoII globular clusters, as derived by Cacciari et al. (2005) and summarized in eqs. (10)–(15) in Zorotovic et al. (2010). Clearly, there is a tendency for most of the ab-type RR Lyrae to fall around the OoI line in this diagram, which again is fully consistent with an OoI classification for the cluster. The RRC's, on the other hand, appear to have shorter periods, at a given amplitude, than indicated by the reference OoI line, which in turn is based on the M3 RR Lyrae (Cacciari et al. 2005), which is consistent with the pattern observed in Figure 6. A possible interpretation for these differences has been provided by Clement & Shelton (1999), who pointed out that, in the period-amplitude diagram, well-behaved RRab stars of different metallicities seemed to follow a fairly universal mean locus, defined solely by their Oosterhoff types, whereas the RRC's, on the contrary, presented systematic deviations towards shorter periods (at a given amplitude) with increasing metallicity. Given that M62 is more metal-rich than M3, this provides a reasonable explanation for our results.

There is, however, one aspect of the M62 variable star population that may not seem immediately compatible with an OoI classification, namely, the number fraction of c-type variables f_c . It has long been thought that the latter quantity is a strong discriminator of Oosterhoff type, with $f_c \simeq 0.17$ for the OoI systems, and $f_c \simeq 0.44$ for OoII systems (see, e.g., Table 3.2 in Smith 1995). In the case of M62, we find $f_c = 0.363$, which is intermediate between these two reference values, but closer to the one for OoII systems. However, as discussed more recently by Catelan et al. (2010, in preparation), f_c is actually *not* a particularly reliable indicator of Oosterhoff type, with known OoI systems covering a wide range in f_c values, from $f_c \approx 0$ up to 0.65 (with most of the objects falling in the range $0.2 \lesssim f_c \lesssim 0.4$), and likewise known OoII systems covering the range from $f_c \approx 0.1$ up to 0.6 (with most of the objects falling in the range $0.3 \lesssim f_c \lesssim 0.55$). We thus conclude that the f_c value for M62 is not inconsistent with an OoI type classification for the cluster; the fact that it is slightly larger than for most OoI systems is likely due to the fact that M62 also has one of the bluest HB types among OoI globulars.

As discussed by (e.g.) Corwin et al. (2003), the average physical parameters of the c- and ab-type RR Lyrae, as derived on the basis of Fourier decomposition of their light curves, can also provide a useful consistency check of the

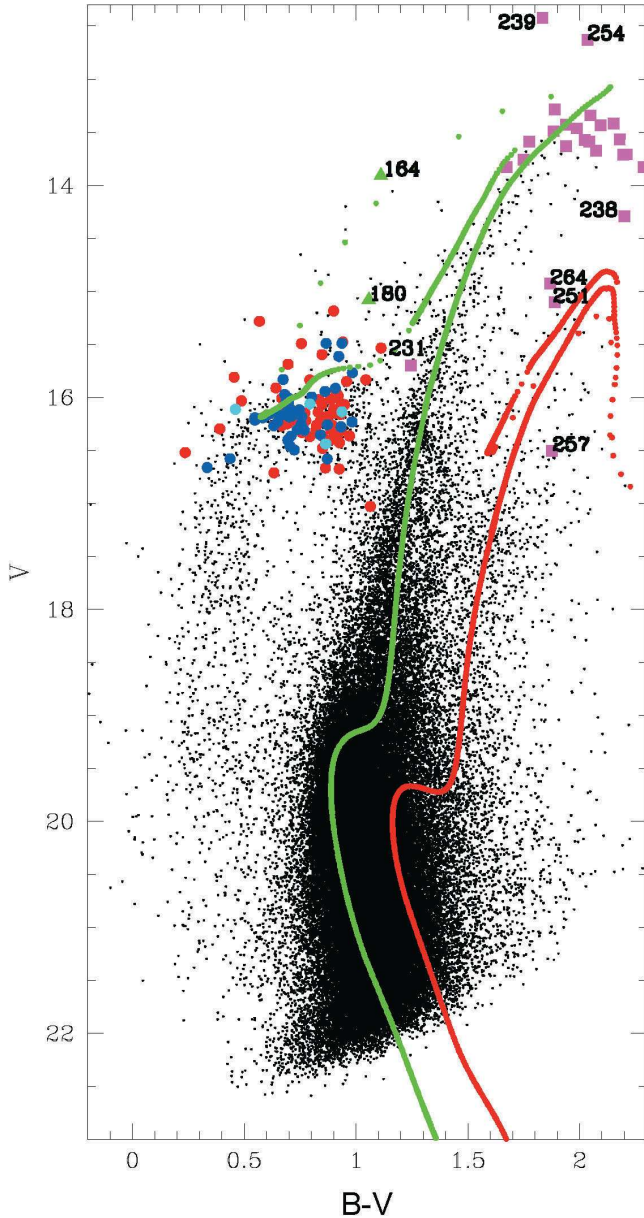


Figure 5. As in Figure 3, but including the variable stars for which the average magnitudes and colors can only be roughly estimated, due to insufficient phase coverage. Filled squares indicate candidate LPV stars. Isochrones for characteristic cluster and bulge chemical compositions are shown as green and red lines, respectively.

derived Oosterhoff type. In Tables 7 and 8 we accordingly compare some of the physical parameters that we derived on the basis of the Fourier decomposition method (§4) with those similarly derived for other clusters in the literature, for the RRC and RRAb stars, respectively. As can be seen from these tables, the Fourier-based physical parameters that we derived for M62 are again entirely consistent with an OoI classification for the cluster.

7. THE A-PARAMETER AND THE HE ABUNDANCE IN M62

Recently, several authors have suggested that He abundance enhancements may be quite commonplace among globular clusters (e.g., D’Antona & Caloi 2008). In this scenario, globular clusters with predominantly blue HB morphologies are suggested to be helium rich, and thus it is worthwhile to check the RR Lyrae stars in M62 in search for evidence of He en-

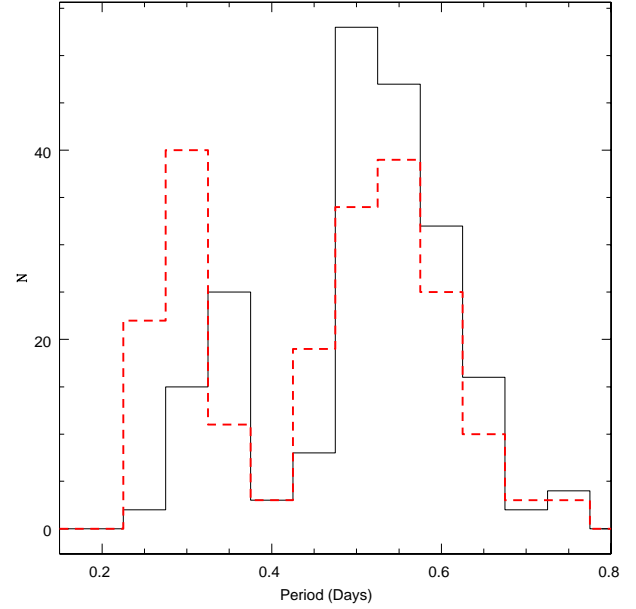


Figure 6. Period histogram for the RR Lyrae stars in M62 (dashed line) and for the RR Lyrae stars in the prototypical OoI globular cluster M3 (solid line).

hancement that might help explain its blue HB.

As is well known, the “A-method” of Caputo & Castellani (1975) can provide strong constraints on the presence (or otherwise) of He enrichment among RR Lyrae stars. From the period-mean density relation of stellar pulsation theory (van Albada & Baker 1971), one finds

$$\log P = 11.497 + 0.84A - 3.481 \log T_{\text{eff}}, \quad (2)$$

where

$$A \equiv \log(L/L_{\odot}) - 0.81 \log(M/M_{\odot}), \quad (3)$$

with the period in days and the temperature in K. Therefore,

$$A = 13.353 - 1.19 \log P - 4.058 \log T_{\text{eff}}. \quad (4)$$

Similarly, on the basis of the more recent models by Caputo, Santolamazza, & Marconi (1998), Cacciari et al. (2005) obtain

$$A = 13.687 - 1.19 \log P - 4.144 \log T_{\text{eff}}. \quad (5)$$

Thus defined, the A-parameter can therefore be easily computed on the basis solely of period measurements and estimates of the stellar temperatures. As already mentioned, this parameter is strongly sensitive to the He abundance; in particular, according to the ZAHB models of Sweigart & Catelan (1998) for $Z = 0.002$, A depends on Y according to $(dA/dY)_{T_{\text{eff}}, Z} \simeq 1.56$, in the range of Y between 0.23 and 0.28. For comparison, the dependence on Z at fixed Y is much milder, the same models indicating, in the range between $Z = 0.0005$ and $Z = 0.002$, a slope $(dA/d \log Z)_{T_{\text{eff}}, Y} \simeq -0.05$.

Here we provide a comparison with the globular cluster M3, which has been extensively studied previously, and which has a metallicity fairly similar to M62’s. In particular, A-parameter values can be derived for the ab-type RR

Table 7
Mean Parameters for RRc Stars in Globular Clusters (from Fourier Decomposition)

| ID | Oo Type | [Fe/H] _{H03} ^a | No. of Stars | M/M_{\odot} | $\log(L/L_{\odot})$ | $T_{\text{eff}}(\text{K})$ | y |
|------------------------------|---------|------------------------------------|--------------|---------------|---------------------|----------------------------|------|
| NGC 6362 ^b | I | -0.95 | 14 | 0.53 | 1.66 | 7429 | 0.29 |
| NGC 6171 (M107) ^c | I | -1.04 | 6 | 0.53 | 1.65 | 7447 | 0.29 |
| NGC 5904 (M5) ^d | I | -1.27 | 14 | 0.54 | 1.69 | 7353 | 0.28 |
| NGC 6266 (M62) | I | -1.29 | 21 | 0.53 | 1.66 | 7413 | 0.29 |
| NGC 6229 ^e | I | -1.43 | 9 | 0.56 | 1.69 | 7332 | 0.28 |
| NGC 6934 ^f | I | -1.54 | 4 | 0.63 | 1.72 | 7290 | 0.27 |
| NGC 5272 (M3) ^g | I | -1.57 | 5 | 0.59 | 1.71 | 7315 | 0.27 |
| NGC 7089 (M2) ^h | II | -1.62 | 2 | 0.54 | 1.74 | 7215 | 0.27 |
| NGC 5286 ⁱ | II | -1.67 | 12 | 0.60 | 1.72 | 7276 | 0.27 |
| NGC 6809 (M55) ^j | II | -1.81 | 5 | 0.53 | 1.75 | 7193 | 0.27 |
| NGC 4147 ^k | I | -1.83 | 9 | 0.55 | 1.69 | 7335 | 0.28 |
| NGC 2298 ^l | II | -1.85 | 2 | 0.59 | 1.75 | 7200 | 0.26 |
| NGC 4590 (M68) ^m | II | -2.06 | 16 | 0.70 | 1.79 | 7145 | 0.25 |
| NGC 7078 (M15) ⁿ | II | -2.26 | 8 | 0.76 | 1.81 | 7112 | 0.24 |
| NGC 6341 (M92) ^o | II | -2.28 | 3 | 0.64 | 1.77 | 7186 | 0.26 |

^a From the Harris (1996) catalog (Feb. 2003 issue).

^b From Olech et al. (2001).

^c From Kaluzny et al. (2000).

^d From Kaluzny et al. (2000).

^e From Borissova et al. (2001).

^f From Kaluzny et al. (2001).

^g From Kaluzny et al. (1998).

^h From Lázaro et al. (2006).

ⁱ From Zorotovic et al. (2010).

^j From Olech et al. (1999).

^k From Arellano Ferro et al. (2004).

^l From Clement et al. (1995).

^m From Clement & Shelton (1997).

ⁿ From Arellano Ferro et al. (2006).

^o From Lázaro et al. (2006).

Table 8
Mean Physical Parameters for RRab Stars in Globular Clusters (from Fourier Decomposition)^a

| ID | Oo Type | [Fe/H] _{H03} | No. of Stars | [Fe/H] _{ZW84} | [Fe/H] _{J95} | $T_{\text{eff}}^{(V-K)}(\text{K})$ | M_V |
|-----------------------|---------|-----------------------|--------------|------------------------|-----------------------|------------------------------------|-------|
| NGC 6362 | I | -0.95 | 14 | -1.26 | -0.93 | 6555 | 0.86 |
| NGC 6171 (M107) | I | -1.04 | 3 | -1.25 | -0.91 | 6619 | 0.85 |
| NGC 1851 ^b | I | -1.22 | 7 | -1.43 | -1.17 | 6494 | 0.80 |
| NGC 5904 (M5) | I | -1.27 | 26 | -1.47 | -1.23 | 6465 | 0.81 |
| NGC 6266 (M62) | I | -1.29 | 39 | -1.31 | -0.99 | 6501 | 0.83 |
| NGC 6229 | I | -1.43 | 9 | -1.60 | -1.41 | 6383 | 0.81 |
| NGC 6934 | I | -1.54 | 24 | -1.53 | -1.31 | 6455 | 0.81 |
| NGC 5272 (M3) | I | -1.57 | 17 | -1.60 | -1.42 | 6438 | 0.78 |
| NGC 7089 (M2) | II | -1.62 | 9 | -1.64 | -1.47 | 6276 | 0.71 |
| NGC 5286 | II | -1.67 | 12 | -1.68 | -1.52 | 6266 | 0.72 |
| NGC 6809 (M55) | II | -1.81 | 3 | -1.77 | -1.65 | 6333 | 0.67 |
| NGC 4147 | I | -1.83 | 5 | -1.46 | -1.22 | 6633 | 0.80 |
| NGC 7078 (M15) | II | -2.26 | 11 | -1.92 | -1.87 | 6237 | 0.67 |
| NGC 6341 (M92) | II | -2.28 | 5 | -1.92 | -1.87 | 6160 | 0.67 |

^a References are the same as in Table 7, except as noted.

^b From Kaluzny et al. (2000).

Lyrae stars in M3, based on the temperatures derived by Kaluzny et al. (1998) from their Fourier decomposition of the V -band light curves. Their procedure is essentially identical to the one adopted in our paper to derive the temperatures listed in the last column of Table 6, and thus A -parameter values for M62 RR Lyrae derived on the basis of these temperatures can be directly compared with those for M3 RR Lyrae stars, based on the temperatures derived by Kaluzny and co-workers. As a result, we find for M3 a $\langle A \rangle = 1.803 \pm 0.023$, and for M62 a $\langle A \rangle = 1.806 \pm 0.024$, implying a difference of $\Delta A = 0.003 \pm 0.033$ between M62 and M3. (The standard deviation of the means are indicated.) If due to a difference in He abundance, these values suggest that M62 is more He-rich

than M3, but by only about 0.002 in Y . Within the errors, this comparison suggests that the RR Lyrae stars in M3 and M62 have closely the same He abundance.

On the other hand, the fact that the average A values are closely the same for both M3 and M62 does not necessarily imply that, at any given temperature, no offset between the two clusters in present. To check for the presence of such possible offsets, we compare in Figure 8 the derived distributions. Intriguingly, and in contrast with what was found in Figure 7,⁷

⁷ Recall that the reference OoI line in Figure 7, from Cacciari et al. (2005), indicates the locus occupied by the presumably “unevolved” RR Lyrae stars in M3.

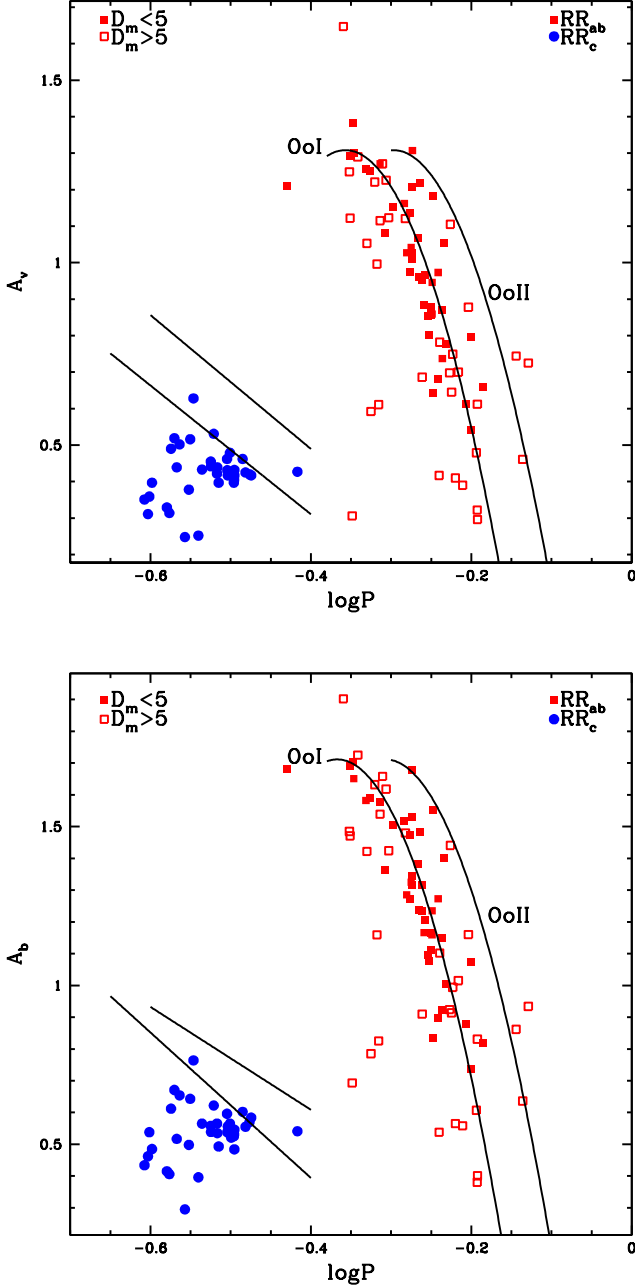


Figure 7. Bailey (period-amplitude) diagram for the RR Lyrae stars in M62, compared with reference lines for RR Lyrae stars in OoI and OoII globular clusters. Top: $A_B - \log P$ diagram; bottom: $A_V - \log P$ plane.

there does appear to be an offset between the two clusters, with the deviation of M62 datapoints from the M3 regression line in the $A - T_{\text{eff}}$ plane (solid line in Fig. 8) amounting to $\Delta A_{T_{\text{eff}}} = 0.020 \pm 0.012$. If due to a difference in He abundance, this would imply that the M62 RR Lyrae stars are more He-rich than their M3 counterparts, by about 0.013 ± 0.008 in Y . This result is confirmed if, instead of the Kaluzny et al. (1998) Fourier parameters for M3 RR Lyrae stars we use those more recently derived by Cacciari et al. (2005). Further work on the temperatures of M62 RR Lyrae stars will be required before we are in a position to conclusively settle this issue.

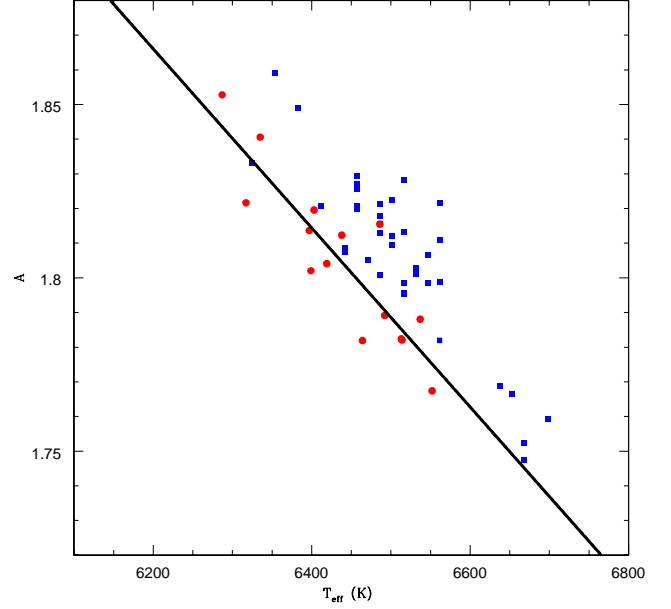


Figure 8. In this figure, A -parameter values, as derived on the basis of equation 3 for ab-type RR Lyrae stars, are plotted as a function of temperature, as derived based on Fourier decomposition ($V-K$ colors). Squares indicate M62 stars, whereas circles represent M3 stars. The straight line is a least-squares fit to the M3 data. See text for more details.

8. SUMMARY

In this paper we have provided a detailed account of the time-series observations that we have collected for the Galactic globular cluster M62, first reported on in Contreras et al. (2005). Our results indicate that M62 is one of the most RR Lyrae-rich (in the sense of total number of RR Lyrae stars present) globular clusters known in the galaxy, and it is actually not unlikely that future studies will reveal that it is *the* most RR Lyrae-rich globular cluster known. In like vein, M62 appears to be the globular cluster with the largest known number of LPV stars in the Milky Way, thus making it a very attractive benchmark object for future RR Lyrae and LPV studies alike.

Discussing the distribution of variable stars in the cluster's CMD, we find that most of the detected variables are likely cluster members. The CMD of the cluster is, however, severely affected by differential reddening; we have accordingly taken benefit of the large number of RR Lyrae variables that are present in the cluster to build a 2-D reddening map for the cluster, which allowed us to present a “corrected” CMD that is much less strongly affected by differential reddening. A full analysis of the cluster CMD will be presented in a forthcoming paper (Contreras et al. 2010, in preparation).

From an analysis of the pulsation periods of the detected RR Lyrae stars, we provide an updated metallicity ($[\text{Fe}/\text{H}]_{\text{ZW84}} = -1.31$, based on Fourier decomposition of the RR Lyrae light curves) and distance modulus $(m-M)_V = 15.58$, based on the recent $M_V(\text{HB}) - [\text{Fe}/\text{H}]$ calibration by Catelan & Cortés (2008) estimates for the cluster. In addition, we discuss a variety of Oosterhoff indicators, including the mean periods, period distribution, and Bailey diagram, and conclude that the cluster is an OoI object, in spite of its blue HB morphology but consistent with its moderately high metallicity. Therefore, metallicity does play an important role in defining Ooster-

hoff type, at least in the case of M62 (see also Contreras et al. 2005). Finally, based on an application of the “A-method,” we conclude that the M62 RR Lyrae stars likely have a similar He abundance as M3, although more work on the temperatures of the M62 RR Lyrae is needed before this result can be conclusively established.

Support for M.C. is provided by MIDEPLAN’s Programa Inicativa Científica Milenio through grant P07-021-F, awarded to The Milky Way Millennium Nucleus; by Proyecto Basal PFB-06/2007; by FONDECYT Regular #1071002. H.A.S. would like to acknowledge the National Science Foundation for support under grants AST0607249 and AST0707756. J.B. acknowledges support from MIDEPLAN’s grant P07-021-F and Proyecto FONDECYT Regular #1080086. We thank an anonymous referee for useful comments that helped improve the presentation of our results.

REFERENCES

- Alard, C. 2000, *A&AS*, 144, 363
- Arellano Ferro, A., Arévalo, M. J., Lázaro, C., Rey, M., Bramich, D. M., & Giridhar, S. 2004, *RevMexAA*, 40, 209
- Arellano Ferro, A., García Lugo, G., & Rosenzweig, P. 2006, *RevMexAA*, 42, 75
- Beccari, G., Ferraro, F. R., Possenti, A., Valenti, E., Origlia, L., & Rood, R. T. 2006, *AJ*, 131, 2551
- Bellazzini, M., Ibata, R., Monaco, L., Martin, N., Irwin, M. J., & Lewis, G. F. 2004, *MNRAS*, 354, 1263
- Blanco, B. M. 1992, *AJ*, 103, 1872
- Bono, G., Caputo, F., & Stellingwerf, R. F. 1995, *ApJS*, 99, 263
- Borissova, J., Catelan, M., & Valchev, T. 2001, *MNRAS*, 324, 77
- Bramich, D. M. 2008, *MNRAS*, 386, L77
- Cacciari, C., Corwin, T. M., & Carney, B. W. 2005, *AJ*, 129, 267
- Caloi, V., Castellani, V., & Piccolo, F. 1987, *A&AS*, 67, 181
- Caputo, F., & Castellani, V. 1975, *Ap&SS*, 38, 39
- Caputo, F., Santolamazza, P., & Marconi, M. 1998, *MNRAS*, 293, 364
- Catelan, M. 2004a, *ApJ*, 600, 409
- Catelan, M. 2004b, in *Variable Stars in the Local Group*, ASP Conf. Ser., 310, ed. D. W. Kurtz & K. R. Pollard (San Francisco: ASP), 113
- Catelan, M. 2007, *RevMexAA Conf. Ser.*, 26, 93
- Catelan, M. 2009, *Ap&SS*, 320, 261
- Catelan, M., & Cortés, C. 2008, *ApJ*, 676, L135
- Catelan, M., & de Freitas Pacheco, J. A. 1993, *AJ*, 106, 1858
- Catelan, M., et al. 2006, *Mem. Soc. Astron. Italiana*, 77, 202
- Clement, C. M., Bezaire, J., & Giguere, D. 1995, *AJ*, 110, 2200
- Clement, C. M., Jankulak, M., & Simon, N. R. 1992, *ApJ*, 395, 192
- Clement, C. M., et al. 2001, *AJ*, 122, 2587
- Clement, C. M., & Shelton, I. 1997, *AJ*, 113, 1711
- Clement, C. M., & Shelton, I. 1999, *ApJ*, 515, L85
- Clementini, G., Corwin, T. M., Carney, B. W., & Sumerel, A. N. 2004, *AJ*, 127, 938
- Clementini, G., et al. 2009, *ApJ*, 704, L103
- Cleveland, W. S. 1979, *J. Amer. Stat. Assoc.*, 74, 829
- Cleveland, W. S., & Devlin, S. J. 1988, *J. Amer. Stat. Assoc.*, 83, 596
- Cocozza, G., Ferraro, F. R., Possenti, A., Beccari, G., Lanzoni, B., Ransom, S., Rood, R. T., & D’Amico, N. 2008, *ApJ*, 679, L105
- Contreras, R., Catelan, M., Smith, H. A., Pritzl, B. J., & Borissova, J. 2005, *ApJ*, 623, L117
- Contreras, R., et al. 2008, *Mem. Soc. Astron. Italiana*, 79, 686
- Corwin, T. M., Catelan, M., Borissova, J., & Smith, H. A. 2004, *A&A*, 421, 667
- Corwin, T. M., Catelan, M., Smith, H. A., Borissova, J., Ferraro, F. R., & Raburn, W. S. 2003, *AJ*, 125, 2543
- Corwin, T. M., Borissova, J., Stetson, P. B., Catelan, M., Smith, H. A., Kurtev, R., & Stephens, A. W. 2008, *AJ*, 135, 1459
- Crane, J. D., Majewski, S. R., Rocha-Pinto, H. J., Frinchaboy, P. M., Skrutskie, M. F., & Law, D. R. 2003, *ApJ*, 594, 119
- D’Antona, F., & Caloi, V. 2008, *MNRAS*, 390, 693
- Deb, S., & Singh, H. P. 2010, *MNRAS*, 402, 691
- Demarque, P., Zinn, R., Lee, Y.-W., & Yi, S. 2000, *AJ*, 119, 1398
- Fiorentino, G., et al. 2010, *ApJ*, 708, 817
- Forbes, D. A., Strader, J., & Brodie, J. P. 2004, *AJ*, 127, 3394
- Gerashchenko, A. N., Kadla, Z. I., & Malakhova, Yu. N. 1997, *IBVS*, 4418, 1
- Harris, W. E. 1996, *AJ*, 112, 1487
- Jurcsik, J. 1995, *AcA*, 45, 653
- Jurcsik, J. 1998, *A&A*, 333, 571
- Jurcsik, J., & Kovács, G. 1996, *A&A*, 312, 111
- Jurcsik, J., & Kovács, G. 1999, *NewA Rev.*, 43, 463
- Kaluzny, J., Hilditch, R. W., Clement, C., & Rucinski, S. M. 1998, *MNRAS*, 296, 347
- Kaluzny, J., Olech, A., & Stanek, K. Z. 2001, *AJ*, 121, 1533
- Kaluzny, J., Olech, A., Thompson, I., Pych, W., Krzeminski, W., & Schwarzenberg-Czerny, A. 2000, *A&AS*, 143, 215
- Kinman, T. D., Saha, A., & Pier, J. R. 2004, *ApJ*, 605, L25
- Kovács, G. 1998, *Mem. Soc. Astron. Italiana*, 69, 49
- Kovács, G., & Jurcsik, J. 1996, *ApJ*, 466, L17
- Kovács, G., & Jurcsik, J. 1997, *A&A*, 322, 218
- Kovács, G., & Kanbur, S. M. 1998, *MNRAS*, 295, 834
- Kovács, G., & Walker, A. R. 1999, *ApJ*, 512, 271
- Kovács, G., & Walker, A. R. 2001, *A&A*, 371, 579
- Kuehn, C., et al. 2008, *ApJ*, 674, L81
- Lafler, J., & Kinman, T. D. 1965, *ApJS*, 11, 216
- Landolt, A. U. 1992, *AJ*, 104, 340
- Lázaro, C., Ferro, A. A., Arévalo, M. J., Bramich, D. M., Giridhar, S., & Poretti, E. 2006, *MNRAS*, 372, 69
- Lee, J.-W., & Carney, B. W. 1999, *AJ*, 118, 1373
- Liller, M. H., & Lichten, S. M. 1978, *AJ*, 83, 41
- Malakhova, Yu. N., Gerashchenko, A. N., & Kadla, Z. I. 1997, *IBVS*, 4457, 1
- Mateu, C., Vivas, A. K., Zinn, R., Miller, L. R., & Abad, C. 2009, *AJ*, 137, 4412
- Mochejska, B. J., Kaluzny, J., Stanek, K. Z., Sasselov, D. D., & Szentgyorgyi, A. H. 2001, *AJ*, 121, 2032
- Moretti, M. I., et al. 2009, *ApJ*, 699, L125
- Morgan, S. M., Wahl, J. N., & Wiecekhorst, R. M. 2007, *MNRAS*, 374, 1421
- Olech, A., Kaluzny, J., Thompson, I. B., Pych, W., Krzeminski, W., & Schwarzenberg-Czerny, A. 1999, *AJ*, 118, 442
- Olech, A., Kaluzny, J., Thompson, I. B., Pych, W., Krzeminski, W., & Schwarzenberg-Czerny, A. 2001, *MNRAS*, 321, 421
- Oosterhoff, P. Th. 1939, *Observatory*, 62, 104
- Oosterhoff, P. Th. 1944, *Bull. Astron. Inst. Neth.*, 10, 55
- Petersen, J. O. 1986, *A&A*, 170, 59
- Piotto, G., et al. 2002, *A&A*, 391, 945
- Pietrinferni, A., Cassisi, S., Salaris, M., & Castelli, F. 2006, *ApJ*, 642, 797
- Possenti, A., D’Amico, N., Manchester, R. N., Camilo, F., Lyne, A. G., Sarkissian, J., & Corongiu, A. 2003, *ApJ*, 599, 475
- Pritzl, B. J., Smith, H. A., Catelan, M., & Sweigart, A. V. 2002, *AJ*, 124, 949; erratum: 2003, *AJ*, 125, 2752
- Pritzl, B. J., Smith, H. A., Stetson, P. B., Catelan, M., Sweigart, A. V., Layden, A. C., & Rich, R. M. 2003, *AJ*, 126, 1381
- Sarajedini, A., Mancone, C. L., Lauer, T. R., Dressler, A., Freedman, W., Trager, S. C., Grillmair, C., & Mighell, K. J. 2009, *AJ*, 138, 184
- Simon, N. R., & Clement, C. M. 1993, *ApJ*, 410, 526
- Simon, N. R., & Teays, T. J. 1982, *ApJ*, 261, 586
- Smith, H. A. 1995, *RR Lyrae Stars* (Cambridge University Press, Cambridge)
- Stellingwerf, R. F. 1978, *ApJ*, 224, 953
- Stellingwerf, R. F., & Donohoe, M. 1987, *ApJ*, 314, 252
- Stetson, P. B. 1987, *PASP*, 99, 191
- Stetson, P. B. 1994, *PASP*, 106, 250
- Suntzeff, N. B., Kinman, T. D., & Kraft, R. P. 1991, *ApJ*, 367, 528
- Sweigart, A. V., & Catelan, M. 1998, *ApJ*, 501, L63
- Tomaney, A. B., & Crotts, A. P. S. 1996, *AJ*, 112, 2872
- Trager, S. C., Djorgovski, S., & King, I. R. 1993, *Structure and Dynamics of Globular Clusters*, ASP Conf. Ser., Vol. 50, ed. S. Djorgovski & G. Meylan (San Francisco: ASP), 347
- Trager, S. C., Djorgovski, S., & King, I. R. 1995, *AJ*, 109, 218; erratum: *AJ*, 109, 218
- van Agt, S. L. T. J., & Oosterhoff, P. T. 1959, *Ann. Sternw. Leiden*, 21, 253
- van Albada, T. S., & Baker, N. 1971, *ApJ*, 169, 311
- Zinn, R., & West, M. J. 1984, *ApJS*, 55, 45
- Zorotovic, M., Catelan, M., Zoccali, M., Pritzl, B. J., Smith, H. A., Stetson, A. W., Contreras, R., & Escobar, M. E. 2009, *AJ*, 137, 257
- Zorotovic, M., et al. 2010, *AJ*, 139, 357

APPENDIX

SAMPLE LIGHT CURVES

Here we show a representative sample of light curves for the newly discovered variable stars in M62. The full set of derived light curves, including our light curves for the previously known variables in the cluster, can be found in the electronic version of this paper.

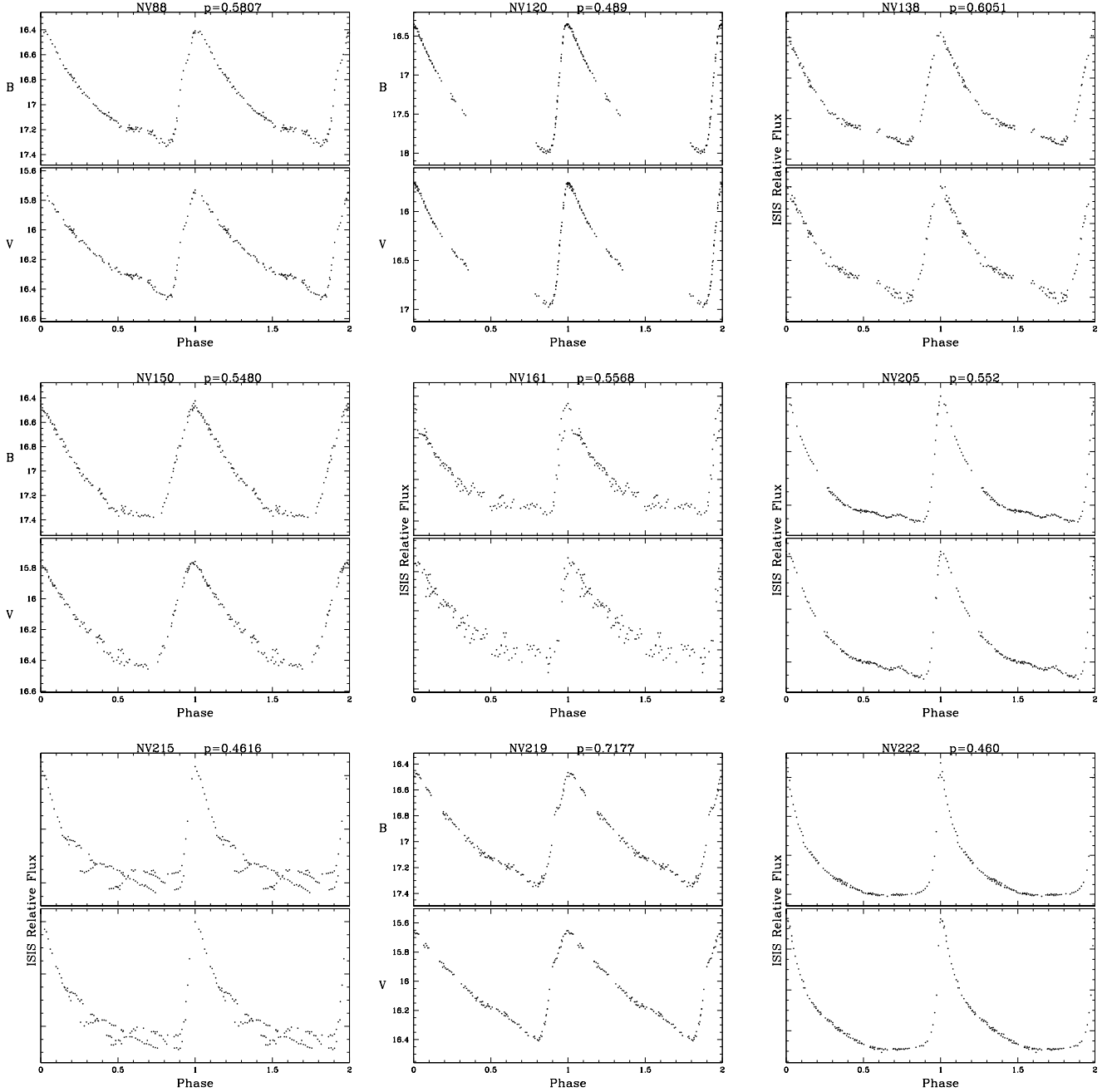


Figure 9. Sample light curves for newly-discovered ab-type RR Lyrae stars. (The full set can be found in the electronic version of this paper.)

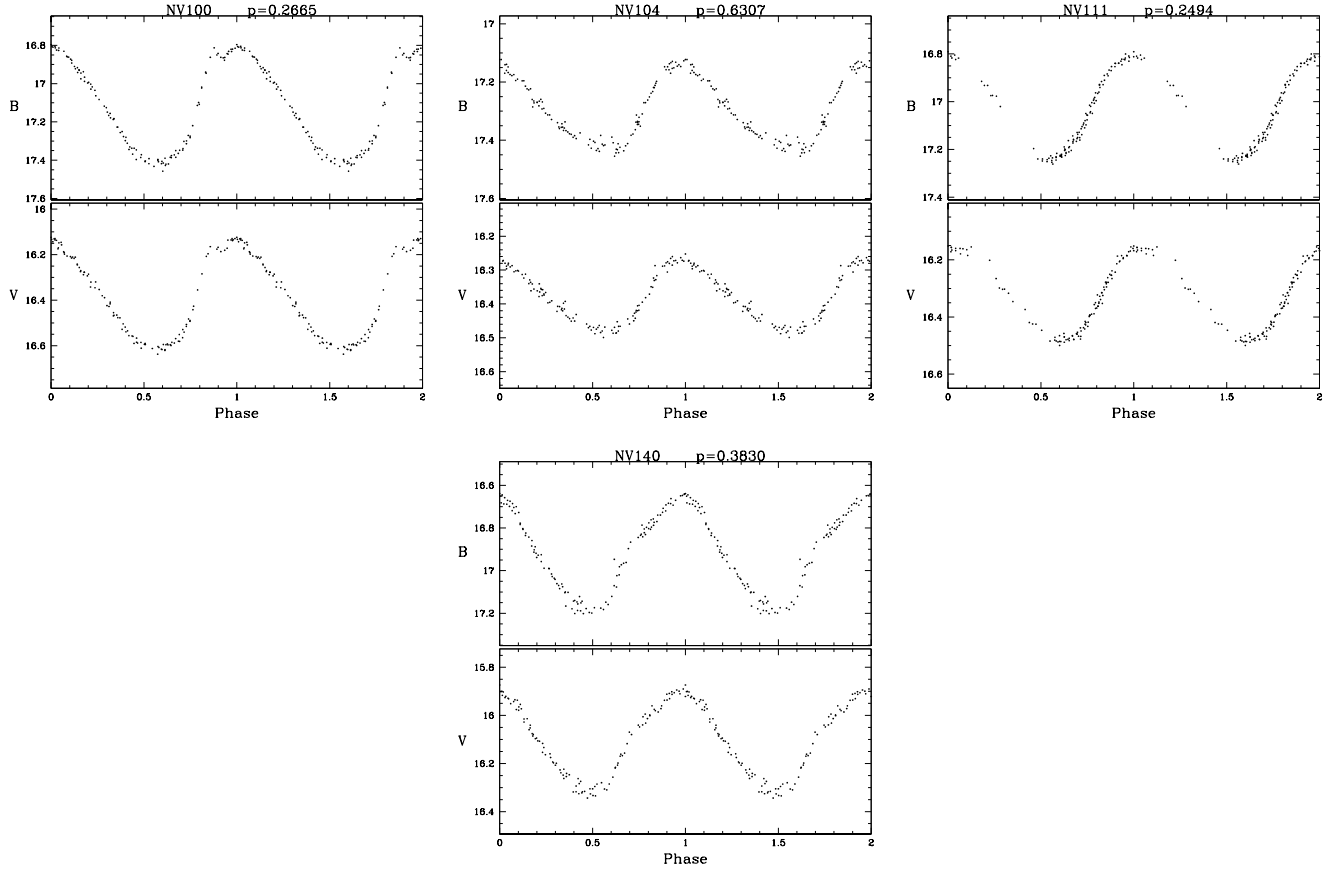


Figure 10. Sample light curves for newly-discovered c-type RR Lyrae stars. (The full set can be found in the electronic version of this paper.)

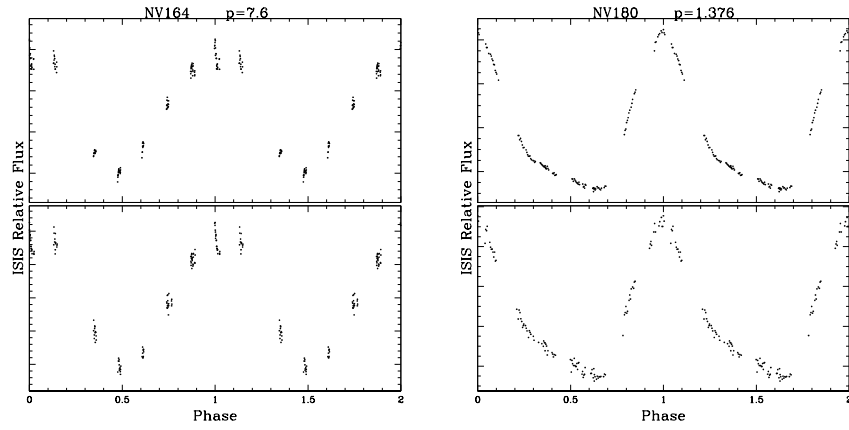


Figure 11. Sample light curves for newly-discovered type II Cepheids. (The full set can be found in the electronic version of this paper.)

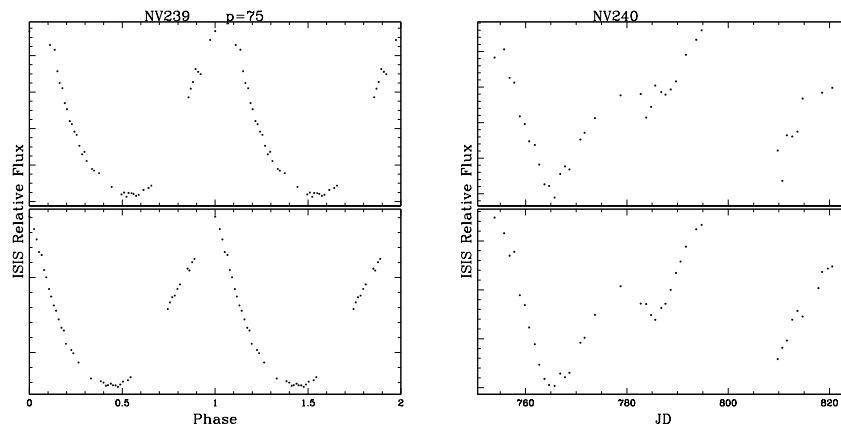


Figure 12. Sample light curves for newly-discovered long-period variables. (The full set can be found in the electronic version of this paper.)

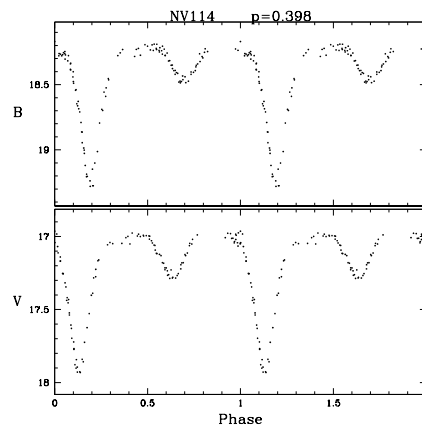


Figure 13. Light curves for NV114, a newly discovered eclipsing binary.

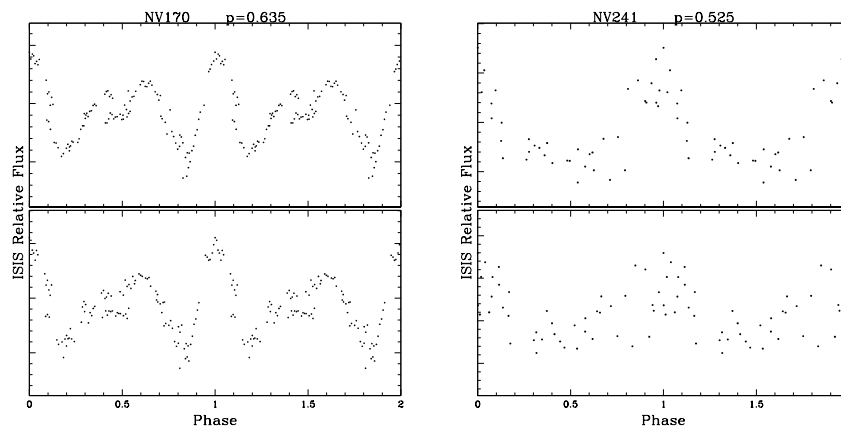


Figure 14. Sample light curves for newly-discovered variable stars whose classification remains unclear. (The full set can be found in the electronic version of this paper.)